# Towards understanding the effect of fibrinogen interactions on fibrin gel structure

Anna C. Nelson o

Department of Mathematics, Duke University, Box 90320, Durham, North Carolina 27708-0320, USA

# Aaron L. Fogelson<sup>†</sup>

Departments of Mathematics and Biomedical Engineering, University of Utah, 155 South 1400 East, Room 233, Salt Lake City, Utah 84112-0090, USA

(Received 24 February 2022; revised 22 November 2022; accepted 23 January 2023; published 21 February 2023)

Fibrin gelation involves the enzymatic conversion of the plasma protein fibrinogen to fibrin monomers which then polymerize to form the gel that is a major structural component of a blood clot. Because fibrinogen provides the material from which fibrin is made, it is generally regarded as promoting the gelation process. However, fibringen can bind to a site on a fibrin oligomer, preventing another fibrin oligomer from binding there, thus slowing the polymerization process. "Soluble fibrin oligomers," which are mixtures of fibrin and fibrinogen, are found in the blood plasma and serve as biomarkers for various clotting disorders, so understanding the interplay between fibrin and fibrinogen during fibrin polymerization may have medical importance. We present a kinetic gelation model of fibrin polymerization which accounts for the dual and antagonistic roles of fibrinogen. It builds on our earlier model of fibrin polymerization that proposed a novel mechanism for branch formation, which is a necessary component of gelation. This previous model captured salient experimental observations regarding the determinants of the structure of the gel, but did not include fibrinogen binding. Here, we add to that model reactions between fibrinogen and fibrin, so oligomers are now mixtures of fibrin and fibrinogen, and characterizing their dynamics leads to equations of substantially greater complexity than previously. Using a moment generating function approach, we derive a closed system of moment equations and we track their dynamics until the finite time blow-up of specific second moments indicates that a gel has formed. In simulations begun with an initial mixture of fibrin and fibrinogen monomers, a sufficiently high relative concentration of fibringen prevents gelation; the critical concentration increases with the branch formation rate. In simulations begun with only fibrinogen monomers that are converted to fibrin at a specified rate, the rates of conversion, fibringen binding to oligomers, and branch formation together determine whether a gel forms, how long it takes to form, and the structural properties of the gel that results.

## DOI: 10.1103/PhysRevE.107.024413

### I. INTRODUCTION

An important constituent of blood clots is a fibrous mesh composed of the protein fibrin. Fibrin is produced by the action of the coagulation enzyme thrombin on the soluble precursor molecule fibrinogen that is present in high concentration in the blood plasma. The insoluble fibrin mesh is a branched polymer structure in the formation of which no specific branch forming or inducing molecule is involved. The structure of the fibrin mesh has important health implications as it affects the mechanical properties of the clot (its strength and flexibility) and it also affects the efficacy of the fibrinolytic process which breaks down the clot [1,2]. A highly ramified gel can be formed in vitro in mixtures of thrombin and fibrinogen alone (in a suitable ionic environment). In vitro, it is seen that the thrombin concentration influences the fibrin gel's structure; a high thrombin concentration leads to a "fine" clot with a high number density of branch points and relatively thin fibers, while a low thrombin concentration leads

to a "coarse" clot with a low number density of branch points and relatively thick fibers [1,3]. It is believed that the fibrin gel structure is kinetically determined, but the regulation of fibrin branch formation remains largely a mystery.

Fibrinogen is an elongated molecule with a central domain and two identical end domains. During fibrin polymerization, thrombin cleaves two short polypeptide chains on the central domain exposing two "A-knob" binding sites and thereby producing fibrin monomers. An A-knob binding site of one fibrin monomer can bind to a constitutively active binding site, an "a-hole," present in the distal domain of a fibrinogen monomer or a different fibrin monomer. Such binding among fibrin molecules leads to longitudinal growth and produces half-staggered fibrin structures called protofibrils. When a protofibril reaches a critical length, it can bind side-to-side to other long protofibrils in a process called lateral aggregation, producing thicker fibrin fibers. During the overall polymerization process, a branched structure forms that results in a three-dimensional network of fibrin fibers, which appears at a time referred to as the gel point or gel time [4]. While the branching process remains poorly understood, it is known that the structure of the branched network is mostly determined by gel time [5] and that the structure

<sup>\*</sup>Corresponding author: anelson@math.duke.edu

<sup>†</sup>fogelson@math.utah.edu

depends on the concentration of thrombin as discussed above [3]. The binding together of two fibrin monomers can be thought of as occurring in two steps, first the a-hole of one molecule binds to the A-knob of the other, and then the a-hole of the second molecule binds to the A-knob of the first.

We previously published a model of fibrin polymerization which builds upon the two-step binding process and incorporates a plausible branch formation mechanism. We showed that the model displayed the experimentally observed qualitative behavior in terms of branch point density [6]. To our knowledge, this is the only existing model that includes a mechanism for branch formation during fibrin polymerization. In the original model, fibrin monomers were supplied either initially or at a prescribed rate. In further developments of the model [7,8], fibrin monomers were produced from fibrinogen monomers by thrombin and the gel structure varied with the thrombin concentration as seen experimentally. In these studies, fibrinogen, which alone cannot polymerize, played no role other than as the raw material from which fibrin was made.

In reality, fibrinogen has another role; it can bind to a fibrin oligomer, but its binding is partial and hinders further growth of the oligomer [9-12]. If the bound fibringen is later converted to fibrin by thrombin, then its binding in the oligomer can be completed, removing this hindrance. During the early stages of fibrin polymerization, fibrinogen is generally present at much higher concentration than are fibrin monomers and so fibrinogen-fibrin reactions are expected to be frequent. This situation persists longer when the thrombin concentration is low and, consequently fibrin monomer formation is slow. The novelty of the current paper is our formulation of a model which adds to the model in Ref. [6] the binding of fibrinogen to fibrin oligomers as well as the thrombin-mediated conversion of fibrinogen to fibrin. We use this model to examine how the additional role of fibrinogen affects the dynamics of the oligomer distributions and the structure of the resulting gel if, indeed, a gel forms. The new model is substantially more complex than our existing fibrin-branching model, which tracked only the concentrations of oligomers of differing size and number of branches. In our new model, oligomers are characterized by differing size, number of branches, and differing fibrinogen content. Our new model is an example (albeit a complex one) of a kinetic gelation model of the type pioneered by Ziff and coworkers [13] and it helps our discussion to briefly sketch Ziff's work and some related concepts below.

In the Ziff framework, reactions occur among a collection of identical monomers, each of which has f reactive sites. Such monomers are said to have "functionality" f. The monomers can react with one another to form oligomers, and oligomers can react with one another to form even larger oligomers. An oligomer is called a "k-mer" if it is composed of k monomers. Ziff's model follows the time evolution of the concentrations  $c_k$  of k-mers as oligomers interact through a single type of reaction in which a reactive site on one oligomer binds to a reactive site on a different oligomer. In the Ziff model, a k-mer has (f - 2)k + 2 free reactive sites and it is assumed that k-mers react with j-mers at a rate proportional to the product of the concentrations of free reactive sites

on each of these types of oligomers, i.e., in proportion to  $[(f-2)k+2]c_k[(f-2)j+2]c_j$ .

Ziff explored the question of whether a gel forms and, if so, when it forms. Informally, the gel is a "treelike oligomer of infinite size" and a precise mathematical definition is given below. Whether and how fast a gel forms in Ziff's model depends on the integer value of the functionality f; a gel forms if and only if f > 3 and it forms more quickly for larger values of f. The actual mathematical condition for gel formation is f > 2; this condition is relevant in our fibrin-fibrinogen model where we look at a quantity we call the "average functionality" which needs not be integer valued.

The oligomer distribution in the Ziff model has zeroth, first, and second moments  $M_0 = \int_k c_k$ ,  $M_1 = \int_k kc_k$  and  $_{k}k^{2}c_{k}$ , respectively. From these moments, two different useful averages can be formed,  $a_n = M_1/M_0$  and  $a_w =$  $M_2/M_1$  which sometimes are called the "number-average mass" and "weight-average mass," respectively [14]. The number-average mass is based on sampling a k-mer with a probability  $c_k/M_0$  that is determined by the relative number of k-mers in the mix of oligomers. The weight-average mass is based on sampling k-mers with probability  $kc_k/M_1$ , so that a kmer is sampled with a probability that is proportional to both its size and its relative frequency in the oligomer mixture. For a weight-average mass, large oligomers contribute more to the average than do small ones, more so when the ratio of the large oligomer size to the small oligomer size grows larger. Ziff's definition of gel formation is that the weight-average mass  $M_2/M_1$  blows up in finite time, and the time of blow up is called the gel time. As stated above, in Ziff's model, this average blows up in finite time if and only if f > 2.

The number-average is useful in describing the potential of an oligomer to participate in a chemical reaction with another oligomer. For two specific oligomers, the rate at which they react with one another depends on the number of free reaction sites of each of them, and not directly on the number of monomers comprising them. We define the average functionality as the number-average of the number of reaction sites on the various oligomers: {  $_{k}[(f-2)k+2]c_{k}]/M_{0}$ . In Ziff's model, the average functionality increases with every reaction, and so it is always larger than the prescribed functionality f of the monomers in that model. As we describe below, fibrinogen and fibrin monomers in our model have functionality 2. The formation of a branch from three monomers produces a cluster with functionality 3, and it is only through sufficient branch formation that a gel can form. Some reactions in our model, including branch formation, increase the number-average functionality  $f_A$  of oligomers, but the binding of fibrinogen to an oligomer always reduces  $f_A$ . The relative frequency of average-functionality-increasing reactions and averagefunctionality-decreasing reactions influences whether a gel forms in our model and affects the gel's structure if one forms.

There are relatively few previous models of fibrin gelation. Some of the existing models use polymer distribution theory [15] while others take a kinetic, mean field approach to study protofibril formation and the aggregation of protofibrils into fibers [16]. Other models of fibrin polymerization directly use the Ziff model and assumed a functionality greater than 2 so that the model equations have built into them the abil-ity to form a gel [17–19]. Therefore, branch formation is

neither required or even defined. Various subprocesses of fibrin polymerization have been investigated using mathematical modeling. This work includes modeling the conversion of fibrinogen to fibrin [20] and use of single-molecule scale molecular dynamics simulations and many-body dissipative particle dynamics to examine early-time dynamics [21,22]. For more information about these models, see Ref. [23].

As discussed above, we have taken a kinetic gelation model approach to develop a model of fibrin polymerization that includes a mechanism for branch formation [6] and which displays behaviors qualitatively like those seen experimentally [3]. That model and its extensions [8,24] did not include the binding of fibrinogen to fibrin oligomers, which is the main focus of the current paper. Others have published models involving fibrinogen and fibrin interactions [25–27] but these models focus on early events and track only small oligomers; they do not track branch formation or other quantities related related to gel structure. In fact, none allow for gelation to occur.

To investigate the multiple roles of fibrinogen in fibrin polymerization, we herein present a two-monomer kinetic polymerization model which involves two distinct types of monomers, denoted M and  $\hat{M}$ , that represent fibrin and fibrinogen, respectively. Each monomer has two reaction sites but the reactions in which the M binding sites can participate differ from those for the  $\hat{M}$  sites. The model includes five types of reactions that represent those that occur during fibrin polymerization prior to gelation. In the model, larger oligomers are formed through reactions between reaction sites on smaller oligomers and can be composed of mixtures of M and M. As in the Ziff framework, each reaction occurs at a rate proportional to the product of the concentrations of the types of free reaction sites involved in that reaction. Our model tracks concentrations of oligomers of all possible types using an infinite set of ordinary differential equations.

As in Refs. [6,13,28], we introduce a moment generating function and obtain a single partial differential equation, from which we derive a *closed* system of ODEs for the lower order moments of the oligomer distribution. We can use the moment system until a finite time blow-up in one or more of the oligomer distribution's second moments occurs. This blow-up event is interpreted as gelation as it corresponds to the weight-average oligomer size approaching infinity in finite time. If gelation occurs, then the weight-average branch concentration and reaction site concentration also blow up. The result is the presence of at least one oligomer whose size, number of branches, and number of reaction sites increases without bound, a situation corresponding to an intuitive notion of gel formation.

The remainder of the paper is organized as follows: We first sketch the development of our model (with details given in Appendix A). We then examine its behavior in three cases, each motivated by a possible biological situation. In this paper, we do not make comparisons of our results with specific experimental observations, as some of the rate constants in our model remain to be determined. Instead our intent is to characterize the range of behaviors of the new model, in particular looking at the effect of fibrinogen binding on gel formation and structure and to understand those behaviors in terms of the relative rates of the various processes included in the model.

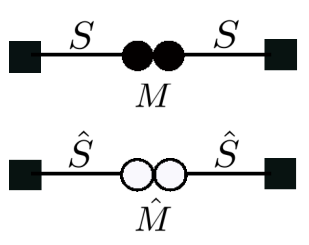


FIG. 1. Schematic of monomers. Monomer M and monomer  $\hat{M}$  with S and  $\hat{S}$  half-domains, respectively.

#### II. FIBRINOGEN-FIBRIN BRANCHING MODEL

Here, we introduce the fibrinogen-fibrin branching model. It extends the branching model found in Ref. [6] to include fibrinogen binding and conversion of fibrinogen to fibrin using a framework similar to Refs. [13,28]. We idealize a fibrin monomer, M, to be a linear molecule consisting of two half-domains, S. An M monomer has two kinds of binding sites, one at each of its ends and two in the center, corresponding to "a-holes" and "A-knobs," respectively. We depict these respective binding sites as squares and circles in Figs. 1 and 2(c). For brevity, we refer to these as square sites and circle sites. We allow a circle site of one M monomer to bind to a square site of another M monomer. We also introduce an idealized fibrinogen monomer,  $\hat{M}$ , as a linear molecule consisting of two-half domains  $\hat{S}$  (see Fig. 1). The square binding site

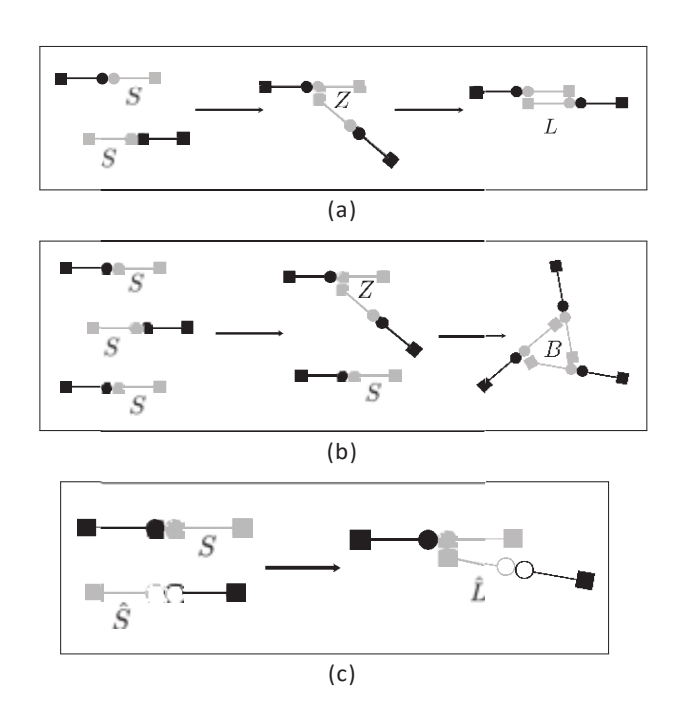


FIG. 2. Schematic of binding reactions in fibrinogen-fibrin branching model. The linking reaction in panel (a) and the binding reaction in panel (b) involve only M monomers that represent fibrin and are identical to reactions in Ref. [6]. The reaction in panel (c) involves an M monomer and an M monomer representing fibrinogen and results in the occupation of an S domain. The dangling S domain cannot interact with any other species. (a) Link formation with M-type monomers. (b) Branch formation process with M-type monomers. (c)  $\hat{M}$ -type monomer binding to M-type monomer, occupying an S domain.



FIG. 3. Schematic of oligomer,  $C_{120}$ . A trimer consisting of one M and two  $\hat{M}$  monomers, representing a heterogeneous trimer with two free fibringen reaction sites and no free fibrin reaction sites.

on an  $\hat{S}$  domain can bind to a circle S binding site on a fibrin molecule, but not to sites on other  $\hat{S}$  domains.

The model includes two types of reactions involving only M monomers. We imagine that linear polymerization begins with a square binding site on a monomer's S domain binding to a circle binding site on a different monomer's S domain, forming the intermediate species Z so that  $S + S \rightarrow Z$ . This molecule can then "zipper" closed to form a linear link L [see Fig. 2(a)]. Letting [S] denote the concentration of S domains on M monomers and assuming the law of mass action, the initial binding event occurs at rate  $k_s[S]^2$  and the overall reaction  $S + S \rightarrow L$  occurs at rate  $k_s k_z[S]^2 = k_l[S]^2$ , where  $k_z$  is the rate constant for zippering events and  $k_l$  is the rate constant for the overall reaction. In the model, we consider only the overall bimolecular reaction in which two S domains join to form a link with rate constant  $k_l = k_s k_z$ .

Due to the two-step nature of linear polymerization, the process of zippering can be blocked by another S domain binding event, resulting in a structure we call a branch (B) [see Fig. 2(b)]. The rate constant for branch formation between a Z structure and an S domain is  $k_B[S]$ , so the overall rate of branch formation is  $k_b[S]$ , where  $k_b = k_B k_s$ . The model involves only the overall trimolecular branching reaction S + S $+ S \rightarrow B$ . While higher-order branch structures can in principle form, considering them does not lead to greater insight and they are not included in the analysis below.

We also allow reactions that involve  $\hat{M}$  monomers. The square binding site on a  $\hat{S}$  domain can bind to a circle binding site on a S domain, as shown in Fig. 2(c), at rate  $k_g[\hat{S}][S]$  to form species L. To reflect the fact that "A-knobs" on fibrinogen have not been removed, we assume that the open circle on an S domain cannot completely bind to the square on the S domain. If another M monomer binds to the other S domain on L, then species  $C_{120}$  (shown in Fig. 3) is formed. It cannot participate in any binding reactions.

We allow fibringen monomers to bind to free fibrin binding sites in fibrin monomers or larger oligomers, but, as explained below, we do not allow binding of a fibringen that is already part of an oligomer. Finally, we allow conversion of an M fibringen monomer to an M fibrin monomer with rate constant  $k_m$  and we allow conversion of fibrinogen in an oligomer to fibrin with rate constant  $k_o$ . We assume that the newly-converted fibrin in oligomer immediately completes the zippering process halted earlier to form a linear link. In a model that explicitly includes the enzyme thrombin, the rates  $k_m$  and  $k_o$  would be proportional to the instantaneous thrombin concentration. In this paper, we treat  $k_m$  and  $k_o$  as constant, as if the thrombin concentration itself were constant.

Taking into account the above reactions, we next describe the formation of clusters. We define cluster  $C_{mgk}$  to be composed of m + 2(g + k - 2) fibrin monomers, and to have g free fibrinogen binding sites and k free fibrin binding sites;

we denote the concentration of such clusters by  $c_{mgk}$ . A fibrin monomer (M) is denoted  $C_{102}$  and a fibrinogen monomer (M)by  $C_{020}$ . As discussed above, we assume that when an M monomer binds to a free S domain, the S domain becomes unavailable to bind to anything else. The number of branches in an oligomer can be computed easily using the relation b= k + g - 2.

As noted above, we do not allow fibringen in an oligomer to bind. Our main reason is our desire to limit the mathematical complexity of the model. If we allow such reactions, then the number of fibrinogen in an oligomer would no longer have to equal the number of free fibringen binding sites on the oligomer. Hence, it would be necessary to track oligomers with four distinct attributes rather than three as in the current model. We offer two arguments to support our assumption: (i) At any given time during a simulation, the total concentration of free fibringen binding sites on oligomers is typically much less than the total concentration of free fibrin binding sites and free binding sites on fibringen monomers, so that a fibrin binding site is much more likely to bind with another fibrin binding site or a monomeric fibringen binding site than with a fibrinogen in an oligomer. (ii) If an oligomer-bound fibrinogen were to bind to a fibrin binding site, then the result would be a cluster that is functionally similar to one formed through a new linear link. Since only monomeric M can bind to other oligomers,  $C_{020}$  is the only fibrinogen-containing species that can bind via its S domain to a  $C_{mgk}$  oligomer.

In terms of the notation just introduced, we allow the following reactions to occur:

$$C_{m_1g_1k_1} + C_{m_2g_2k_2} \stackrel{k_l}{\to} C_{m_1+m_2,g_1+g_2,k_1+k_2-2},$$
 (1)

$$C_{m_1g_1k_1} + C_{m_2g_2k_2} + C_{m_3g_3k_3} \xrightarrow{k_b}$$

$$C_{m_1+m_2+m_3-2,g_1+g_2+g_3,k_1+k_2+k_3-3}, \qquad (2)$$

$$C_{mgk} + C_{020} \xrightarrow{k_g} C_{m,g+1,k-1},$$
 (3)

$$C_{020} \xrightarrow{k_{w}} C_{102}, \tag{4}$$

$$C_{mgk} \xrightarrow{k_0} C_{m+1,g-1,k+1}. \tag{5}$$

To calculate some quantities of interest, we must sum over all oligomers that contain fibrin, that is oligomers  $C_{mgk}$  with m> 0, g > 0, k > 0. To facilitate describing these quantities we introduce the notation

$$\begin{array}{ccc}
X & X^{\infty} \\
 & = & . \\
m,g,k & {m=1} \\
 & g=0 \\
 & k=0
\end{array}$$
(6)

We track the total concentration of fibrin,  $M_T$ , the total concentration of fibrinogen,  $\hat{M}_T$ , and the total concentration of branches B, using the expressions

$$M_T = {}^{\mathsf{X}} (m + 2g + 2k - 4)c_{mgk},$$
 (7)

$$\hat{M}_T = g c_{mgk} + c_{020},$$
 (8)

$$M_{T} = \begin{cases} X \\ M_{T} = (m + 2g + 2k - 4)c_{mgk}, \end{cases}$$
(7)  

$$\hat{M}_{T} = gc_{mgk} + c_{020},$$
(8)  

$$A_{T} = gc_{mgk} + c_{020},$$
(9)  

$$A_{T} = gc_{mgk} + c_{020},$$
(9)

Following Ziff, we regard gelation as occurring if  $A \rightarrow \infty$ 

at a finite time, which we call the gel time and denote  $t_{gel}$ .

The gel time depends not only on the above reaction rates,

but also on the initial concentrations of fibrinogen and fibrin monomers. In the Ziff model framework, which pertains to a

system of identical monomers each with a fixed functionality

f, a gel can form only if f > 2 [13]. In our model, fibrino-gen and fibrin monomers have functionality f = 2; gelation can

still occur because the branching reaction gives rise to

oligomers with three or more functional sites. The goal of

our analysis below is to determine which parameter values lead to gel formation, and to determine the clot structure

and oligomer distribution at gel time. With the five reactions described above, we write the equations for the oligomer

concentrations  $c_{mgk}$  and for the concentration of fibrinogen

The total concentration of fibrin in oligomers is  $O = M_T - c_{102}$  and similarly the total concentration of fibrinogen in oligomers is  $O = M_T - c_{020}$ . The concentration of free fibrin reaction sites on oligomers is

$$R = \underset{m,g,k}{\mathsf{X}} k c_{mgk},\tag{10}$$

and we define the weight-average number of monomers (fibrin or fibrinogen) per cluster to be

$$A = \frac{\text{i P}_{m,g,k} (m + 2g + 2k - 4 + g)^2 c_{mgk} + c_{020}}{M_T + \hat{M}_T}, \quad (11)$$

where we use the fact that the number of fibrin monomers in a  $C_{mgk}$  oligomer is m + 2(g + k - 2), as noted earlier.

ligomer is m + 2(g + k - 2), as noted earlier. monomers  $c_{020}$  as  $\frac{dc_{mgk}}{dt} = \frac{z}{k_l} \frac{X}{X} k_1 k_2 c_{m_1g_1k_1} c_{m_2g_2k_2} - k_l k c_{mgk} R + \frac{k_b}{6} \frac{X}{k_1 k_2 + k_3 = m + 2} k_1 k_2 k_3 c_{m_1g_1k_1} c_{m_2g_2k_2} c_{m_3g_3k_3} - \frac{k_b}{2} k c_{mgk} R^2$   $\frac{z}{k_1 + k_2 + k_3 = k + 2} \frac{k_1 k_2 k_3 c_{m_1g_1k_1} c_{m_2g_2k_2} c_{m_3g_3k_3} - \frac{k_b}{2} k c_{mgk} R^2$   $\frac{z}{k_1 + k_2 + k_3 = k + 3} \frac{k_1 k_2 k_3 c_{m_1g_1k_1} c_{m_2g_2k_2} c_{m_3g_3k_3} - \frac{k_b}{2} k c_{mgk} R^2$   $\frac{z}{k_1 + k_2 + k_3 = k + 3} \frac{k_1 k_2 k_3 c_{m_1g_1k_1} c_{m_2g_2k_2} c_{m_3g_3k_3} - \frac{k_b}{2} k c_{mgk} R^2$   $\frac{z}{k_1 + k_2 + k_3 = k + 3} \frac{k_1 k_2 k_3 c_{m_1g_1k_1} c_{m_2g_2k_2} c_{m_3g_3k_3} - \frac{k_b}{2} k c_{mgk} R^2$   $\frac{z}{k_1 + k_2 + k_3 = k + 3} \frac{k_1 k_2 k_3 c_{m_1g_1k_1} c_{m_2g_2k_2} c_{m_3g_3k_3} - \frac{k_b}{2} k c_{mgk} R^2$   $\frac{z}{k_1 + k_2 + k_3 = k + 3} \frac{k_1 k_2 k_3 c_{m_1g_1k_1} c_{m_2g_2k_2} c_{m_3g_3k_3} - \frac{k_b}{2} k c_{mgk} R^2$   $\frac{z}{k_1 + k_2 + k_3 = k + 3} \frac{k_1 k_2 k_3 c_{m_1g_1k_1} c_{m_2g_2k_2} c_{m_3g_3k_3} - \frac{k_b}{2} k c_{mgk} R^2$   $\frac{z}{k_1 + k_2 + k_3 = k + 3} \frac{k_1 k_2 k_3 c_{m_1g_1k_1} c_{m_2g_2k_2} c_{m_3g_3k_3} - \frac{k_b}{2} k c_{mgk} R^2$   $\frac{z}{k_1 + k_2 + k_3 = k + 3} \frac{k_1 k_2 k_3 c_{m_1g_1k_1} c_{m_2g_2k_2} c_{m_3g_3k_3} - \frac{k_b}{2} k c_{mgk} R^2$   $\frac{z}{k_1 + k_2 + k_3 = k + 3} \frac{k_1 k_2 k_3 c_{m_1g_1k_1} c_{m_2g_2k_2} c_{m_3g_3k_3} - \frac{k_b}{2} k c_{mgk} R^2$   $\frac{z}{k_1 + k_2 + k_3 = k + 3} \frac{k_1 k_2 k_3 c_{m_1g_1k_1} c_{m_2g_2k_2} c_{m_3g_3k_3} - \frac{k_b}{2} k c_{mgk} R^2$   $\frac{z}{k_1 + k_2 + k_3 = k + 3} \frac{k_1 k_2 k_3 c_{m_1g_1k_1} c_{m_2g_2k_2} c_{m_3g_3k_3} - \frac{k_b}{2} k c_{mgk} R^2$   $\frac{z}{k_1 + k_2 + k_3 = k + 3} \frac{k_1 k_2 k_3 c_{m_1g_1k_1} c_{m_2g_2k_2} c_{m_3g_3k_3} - \frac{k_b}{2} k c_{mgk} R^2$   $\frac{z}{k_1 + k_2 + k_3 = k + 3} \frac{k_1 k_2 k_3 c_{m_1g_1k_1} c_{m_2g_2k_2} c_{m_1g_1k_1} c_{m_2g_2k_2} c_{m_1g_1k_1} c_{m_2g_2k_2} c_{m_1g_1k_1} c_{m_2g_1k_1} c_{m_2g_1k_1} c_{m_2g_1k_1} c_{m_2g_1k_1} c_{m_2g_1k_1} c_{m_2g_1k_1} c_{m_2g_1k_1} c_{m_2g_1k$ 

$$\frac{dc_{020}}{dt} = -2k_g c_{020} R - k_m c_{020},\tag{13}$$

where R is defined by Eq. (10) and satisfies the differential equation

$$\frac{dR}{dt} = -k_l R^2 - \frac{k_b}{2} R^3 - 2k_g c_{020} R + 2k_m c_{020} + k_o \hat{O}.$$
 (14)

Equation (12) holds for m > 1, g > 0, and k > 0. As indicated by the overbraces, the first terms on the right-hand side of Eq. (12) describe the fibrin link formation reactions and the next two terms describe the fibrin branch formation reactions. Such reactions among smaller oligomers can increase the concentration  $c_{mgk}$ , while reactions of  $C_{mgk}$  oligomers with other oligomer decrease  $c_{mgk}$ . These linking and branching reactions are the same as those considered in Ref. [6]. The next two terms describe how fibrinogen binding to oligomers affects  $c_{mgk}$ , and the remaining pairs of terms describe the conversion of oligomeric and monomeric fibrinogen to fibrin. The terms in Eq. (13) describe the binding of fibrinogen monomers to oligomers and the conversion of fibrinogen monomers to fibrin, respectively.

To facilitate our analysis of the behavior of the infinite set of ordinary differential equations in Eqs. (12) and (13), we introduce a generating function G(t, x, y, z),

$$G(t, x, y, z) = X c_{mgk}(t)x^m y^g z^k,$$
 (15)

and find that

$$\frac{\partial G}{\partial t} = \frac{z}{k_l} \frac{\frac{\ln k \text{ formation}}{\partial z}}{\frac{\partial G}{\partial z}} \left\{ \frac{z}{\frac{\text{fibrinogen}}{z}} \right\} \frac{\text{binding}}{\frac{\partial G}{\partial z}} \left\{ \frac{z}{\frac{\partial G}{\partial z}} + 2k_g c_{020}(y - z) \frac{\partial G}{\partial z} \right\} \\
+ \frac{z}{\frac{k_b}{6x^2}} \frac{\frac{\partial G}{\partial z}}{\frac{\partial G}{\partial z}} - \frac{k_b}{2} z \frac{\partial G}{\partial z} R^2 \\
+ \frac{\frac{z}{k_b}}{\frac{\partial G}{\partial z}} \frac{\frac{\partial G}{\partial z}}{\frac{\partial G}{\partial z}} + \frac{\frac{\partial G}{\partial z}}{\frac{\partial G}{\partial z}} \frac{\partial G}{\partial z} \right\} \frac{c_{01}}{\frac{\partial G}{\partial z}} \left\{ \frac{c_{01}}{c_{020}} + \frac{c_{01}}{c_{020}} + \frac{c_{020}}{c_{020}} + \frac{c_{01}}{c_{020}} \frac{c_{020}}{\frac{\partial G}{\partial z}} \right\} = \frac{c_{01}}{c_{020}} \frac{c_{020}}{c_{020}} + \frac{c_{020}}{c_{020}} \frac{c_{02$$

Note that the fibrinogen monomer concentration  $c_{020}$  is not included in the definition of G(t, x, y, z) in Eq. (15). Using G, we define moments

$$M_{abc} = \frac{\partial^{a+b+c} G}{\partial x^a \partial y^b \partial z^c} \Big|_{x=1,y=1,z=1},$$
 (17)

and we write physical quantities of interest in terms of combinations of the moments  $M_{abc}$ . The total concentration of all fibrin and fibrinogen monomers, the branch concentration, the concentration of free fibrin reaction sites, and the weight-average oligomer size, respectively, can be written as

$$M_{T} = X (m + 2g + 2k - 4)c_{mgk}$$

$$= M_{100} + 2M_{010} + 2M_{001} - 4M_{000}, \qquad (18)$$

$$\hat{M}_{T} = gc_{mgk} + c_{020} = M_{010} + c_{020}, \qquad (19)$$

$$B = {\mathsf{X} \atop (k + g - 2)c_{mgk}} = M_{001} + M_{010} - 2M_{000}, \qquad (20)$$

$$R = {\mathsf{X} \atop m,g,k} \atop kc_{mgk} = M_{001}, \qquad (21)$$

and

$$A = \frac{1}{M_T + \hat{M}_T} (M_{200} + 9M_{020} + 4M_{002} + 12M_{011} + 6M_{110} + 4M_{101} - 8M_{100} - 12M_{001} - 15M_{010} + 16M_{000} + c_{020}).$$
 (22)

In Appendix A, we use Eqs. (16) and (17) to derive ODEs for the low-order moments. In Appendix B, we also show that the average oligomer size A is bounded if and only if  $M_{002}$  is bounded and, furthermore,  $M_{002}$  is bounded if and only if all of the moments in Eq. (22) are bounded. Because it is easier to determine when a variable goes to 0 than to determine when a variable blows up, we use a Riccati transformation in Appendix C to define a new variable V, where  $M_{002} - R = -V^0/(k_l + k_b R)V$ , with the property that  $V \rightarrow 0$  at a finite time if and only if  $A \rightarrow \infty$  at the same time. Hence, V becoming zero at a finite time indicates a gel forms at that time.

Appendix C presents the details of the nondimensionalization that yields the nondimensional equations (23)–(29) for the evolution with respect to nondimensional time  $\tau$  of the nondimensional indicator variable v, the nondimensional concentrations of fibrinogen monomers  $\tilde{c}_{020}$ , fibrin monomers  $\tilde{c}_{102}$ , free fibrin reaction sites r, branches b, fibrin in oligomer o, fibringen in oligomer  $\hat{o}$ , and the nondimensional second moments  $m_{011}$ ,  $m_{020}$ , and  $m_{002}$ :

$$\frac{d}{d\tau^{2}} v = - \sum_{k=1}^{\infty} \kappa^{3} - 2\gamma \tilde{c}_{020}r + \eta_{o}(2m_{011} - \hat{o}) \alpha v + \kappa r^{2} - 4\gamma \tilde{c}_{020} + \frac{\alpha^{c} \eta}{\alpha} \frac{dv}{d\tau'}$$
(23)

$$\frac{d\tilde{c}_{020}}{d\tau} = -2\gamma \,\tilde{c}_{020}r - \eta_m \tilde{c}_{020},\tag{24}$$

$$\frac{d\tilde{c}_{102}}{d\tau} = (-2r - \kappa r^2)\tilde{c}_{102} - 4\gamma \,\tilde{c}_{020}\tilde{c}_{102} + \eta_m \tilde{c}_{020}, \qquad (25)$$

$$\frac{dr}{d\tau} = -r^2 - \frac{\kappa}{2}r^3 - 2\gamma \tilde{c}_{020}r + 2\eta_m \tilde{c}_{020} + \eta_o \hat{o}, \qquad (26)$$

$$\frac{db}{d\tau} = \frac{\kappa}{6}r^3,\tag{27}$$

$$\frac{do}{d\tau} = 2\tilde{c}_{102}r + \kappa \tilde{c}_{102}r^2 + 4\gamma \tilde{c}_{102}\tilde{c}_{020} + \eta_o \hat{o}, \qquad (28)$$

$$\frac{d\hat{o}}{d\tau} = 2\gamma \tilde{c}_{020}r - \eta_o \hat{o},\tag{29}$$

$$\begin{split} \frac{d\hat{o}}{d\tau} &= \, 2\gamma \, \tilde{c}_{020} r - \, \eta_o \hat{o}, \\ \mu & \quad \mu \\ \frac{dm_{011}}{d\tau} &= \, (m_{002} - \, r) m_{011} + \, \kappa \, \, m_{002} - \, \frac{1}{2} r \, \, r m_{011} \end{split}$$

+ 
$$2\gamma \tilde{c}_{020}(m_{002} - m_{011}) + \eta_o(m_{020} - m_{011}),$$
 (30)

$$\frac{dm_{020}}{d\tau} = m_{011}^2 + \kappa m_{011}^2 r + 4\gamma \tilde{c}_{020} m_{011} - 2\eta_o m_{020}, \quad (31)$$

TABLE I. Nondimensional parameter values for each case discussed.

Nondimensional parameter	Case 1	Case 2	Case 3
Initial composition $(\varphi)$	0–1	1	1
Branching $(\kappa)$	$10^{-1} - 10^4$	$10^{-1} - 10^4$	$10^{-1} - 10^4$
Fibrinogen binding (y)	$10^{-1} - 10^4$	$10^{-1} - 10^4$	$10^{-1} - 10^4$
Monomeric conversion $(\eta_m)$	0	$10^{-2} - 10^{2}$	$10^{-2} - 10^{2}$
Oligomeric conversion $(\eta_o)$	0	0	$10^{-7} - 10^2$

$$\frac{dm_{002}}{d\tau} = m_{002}^2 - 2m_{002}r + \kappa_1 m_{002}^2 r - m_{002} r^2$$

$$- 4\gamma \tilde{c}_{020} m_{002} + 2\eta_m \tilde{c}_{020} + 2\eta_o m_{011}, \qquad (32)$$

where  $\alpha = 1 + \kappa r$ .

It is useful to define the initial composition variable  $\varphi$  as

$$\varphi = \frac{\tilde{c}_{020}(0)}{\tilde{c}_{020}(0) + \tilde{c}_{102}(0)}.$$
 (33)

 $\varphi$  is the fraction of initial monomers that are fibringen monomers, and we can express the initial conditions for Eqs. (23)–(32) as

$$v(0) = 1, \quad \frac{dv}{d\tau}(0) = 0,$$

$$\tilde{c}_{020}(0) = \varphi, \quad \tilde{c}_{102}(0) = 1 - \varphi,$$

$$r(0) = 2(1 - \varphi), \quad b(0) = 0,$$

$$o(0) = 0, \quad \hat{o}(0) = 0.$$
(34)

## III. RESULTS

For the results in this paper, we simulate Eqs. (23)–(32) for specified values of the initial composition parameter  $\varphi$ and the nondimensional reaction rates  $\kappa$ ,  $\gamma$ ,  $\eta_m$ , and  $\eta_o$  and we determine if and when a gel forms. If gelation occurs, then  $\tau_{gel}$  denotes the nondimensional time at which  $v \to 0$ . If finite time blow-up does not occur and v remains positive, then we solve the equations until time  $\tau_{\text{max}} = 10^{10}$ . We note that our results are not sensitive to changes in  $\tau_{max}$  provided it is sufficiently large. We define  $\tau_{end} = \min(\tau_{max}, \tau_{gel})$ , which gives the end time of a simulation whether or not a gel forms.

Our parameter studies are organized based on various timescales and we show results for three cases as outlined in Table I. Parameter values are chosen to explore the gelation capability of the system, and some parameter values, in particular, the branching rate, are unknown for fibrin polymerization. For Case 1, we allow linking, branching, and fibrinogen binding, but we do not allow any conversion of fibringen to fibrin. Therefore,  $\eta_m = \eta_o = 0$  and we vary the initial mixture parameter  $\varphi$  between 0 and 1. By eliminating the conversion timescales, Case 1 investigates the ability of fibringen to inhibit gelation and affect concentrations of interest, including the branch concentration and the concentration of fibrinogen in oligomer. In Case 2, we allow the same three binding reactions and also incorporate the monomeric conversion timescale, so  $\eta_m = 0$ . Through this case, the ability of fibrinogen to both hinder and enhance gelation is

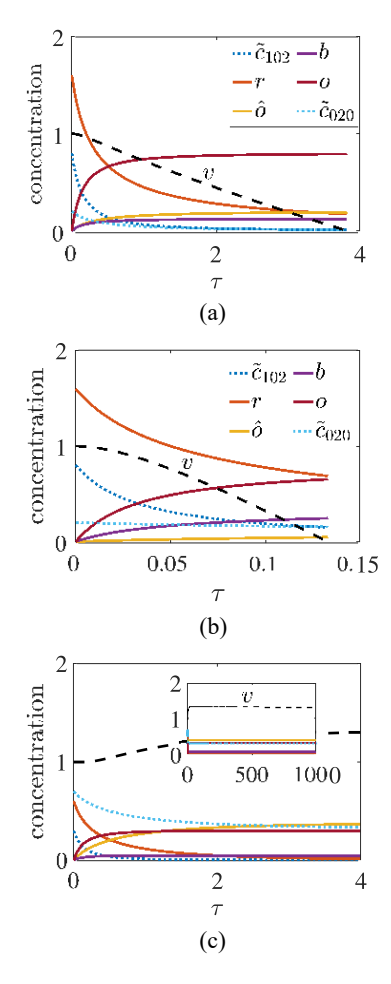


FIG. 4. (Case 1) Time evolution of nondimensional concentrations for varying  $\kappa$  and  $\varphi$  with fixed  $\gamma = 1$ . (a, b) Initial composition parameter  $\varphi = 0.2$ , and (a)  $\kappa = 1$ , (b)  $\kappa = 10$ . (c)  $\kappa = 10$  and  $\varphi = 0.7$ . The inset in panel (c) shows that  $\nu$  remains above 1 at large times.

investigated. In Case 3, we also allow fibrinogen in oligomers to be converted to fibrin, thus representing more closely the biological system. We assume that only fibrinogen monomers are present initially in Cases 2 and 3, so  $\varphi = 1$ .

### A. Case 1: No conversion $(\eta_m = \eta_o = 0)$

With no conversion of fibrinogen, we require  $\varphi$  < 1 for a gel to form, as fibrinogen cannot polymerize by itself. This setup is analogous to an imagined biological experiment in which both fibrinogen and fibrin monomers are present initially and no thrombin is added to the mixture. In our numerical experiments, we determine which values of  $\varphi$  result in gel formation and how fibrinogen binding affects both the gel time and the gel's structure.

We study Eqs. (23)–(32) with  $\eta_m = \eta_o = 0$  until  $v \to 0$  or until  $\tau = \tau_{\text{max}}$ . Figure 4 illustrates how the concentrations of interest evolve in time for different branch rates  $\kappa$  and initial composition parameter values,  $\varphi$ , and for fibrinogen binding rate  $\gamma = 1$ . With  $\varphi = 0.2$ , we compare the situation in which  $\kappa = 1$  [Fig. 4(a)] to that with  $\kappa = 10$  [Fig. 4(b)]. A gel forms sooner for  $\kappa = 10$  than for  $\kappa = 1$ . The concentration

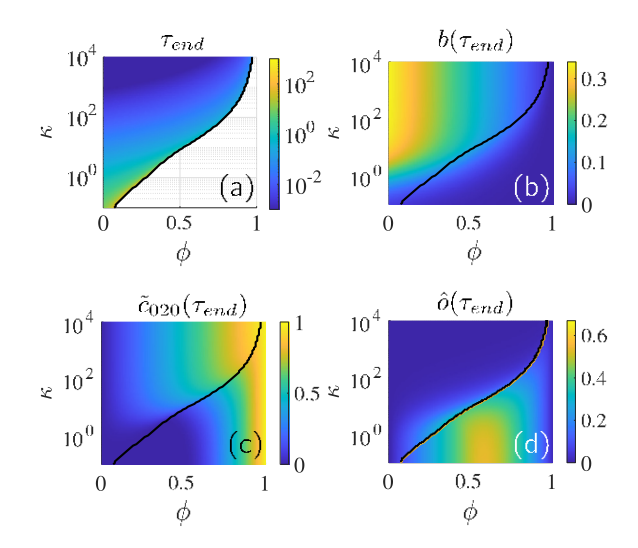


FIG. 5. (Case 1) Results for various branching rates  $\kappa$  and initial composition parameter values  $\varphi$ , with  $\gamma = 1$ . To the left of the black line, a gel forms. (a) Gel times,  $\tau_{\rm gel}$ , and concentrations of (b) branch points b, (c) fibrinogen monomer  $\tilde{c}_{020}$ , and (d) fibrinogen in oligomer  $\hat{o}$  at  $\tau_{\rm end}$ .

of branches at gel time is higher while the concentrations of fibrin in oligomer and fibrinogen in oligomer at gel time are lower for the larger value of  $\kappa$ .

Figure 4 shows concentrations of interest for  $\varphi = 0.7$ , where the proportion of initial fibrinogen has increased compared to Figs. 4(a) and 4(b). Here, a gel does not form, as indicated by the failure of  $\nu$  to approach 0. The inset shows that  $\nu$  remains approximately constant at a value above 1 for over  $10^3$  time units and that the other variables appear to be at steady state. In the main figure, we see that the concentrations of free fibrin reaction sites r and fibrin monomers  $\tilde{c}_{102}$  decay quickly to zero while all of the other concentrations asymptote to positive values. Therefore, the progression to larger oligomers and to gelation is halted by the depletion of free fibrin sites and fibrin monomer.

We show results in Fig. 5 from a parameter exploration to determine whether a gel forms and how concentrations at gel time vary for a range of  $\kappa$  and  $\varphi$  values with  $\gamma=1$ . The heat map color corresponds to either concentration or gel time and where the heat map color is white, no gelation occurs by time  $\tau_{\text{max}}$ . Figure 5(a) shows strong variations in gelation behavior as  $\kappa$  and  $\varphi$  are varied. The black curves in the figure are separatrices between regions in which a gel does or does not form. As  $\kappa$  increases in Fig. 5(a), the upper limit of  $\varphi$  values for which a gel forms also increases. Branching is required for gelation, and as  $\kappa$  increases, the gel time decreases by several orders of magnitude.

In Figs. 5(b), 5(c), and 5(d), the end-time concentrations of branches, fibrinogen monomers, and oligomeric fibrinogen are shown as functions of  $\varphi$  and  $\kappa$ . Figure 5(b) shows that the branch concentration is larger for shorter gel times ( $\varphi$  < 0.2,  $\kappa$  > 30) and that few branches form in the no-gel region. Even though no-gel simulations are continued to time  $\tau_{\text{max}}$ , branch concentrations in the no-gel region at that time are lower than those at  $\tau_{\text{gel}}$  for points in the gel region. These observations are consistent with the results from Fig. 5(d), which show a high

fibrinogen content in oligomers in the no-gel region. Without conversion, fibrinogen binds to an oligomer and permanently occupies a fibrin reactive site, curtailing reactions overall. However, if the branching rate  $\kappa$  is sufficiently large or if  $\varphi$  is small enough, then branch formation can overcome fibrinogen binding thus leading to gelation.

The concentration of fibrinogen monomer,  $\tilde{c}_{020}$  at  $\tau_{\rm end}$  is shown for varying  $\kappa$  in Fig. 5(c). In the no-gel region, there is a lower concentration of fibrinogen monomer for a given  $\varphi$  value than in the gel region. Since no gel forms, fibrino-gen monomer has time to be incorporated into oligomers, resulting in a lower fibrinogen monomer concentration than in the gel region of parameter space. The concentration  $\tilde{c}_{020}$  approaches 1 as  $\varphi \rightarrow$  1. With low or no fibrin, few or no oligomers form and fibrinogen remains largely in monomeric form.

Figure 5(d) demonstrates how the fibringen in oligomer concentration depends on the branching rate and initial composition. Parameters values in the no-gel region produce higher concentrations of oligomeric fibrinogen than those in the gel region, as the free reaction site concentration goes to zero in the no-gel region as time advances (not shown). Interestingly, the largest concentration of fibringen in oligomers occurs for  $\varphi \approx 0.66$ . At this  $\varphi$  value, there are approximately two fibrinogen monomers for every fibrin monomer. For fibringen binding rate  $\gamma = 1$  or higher, many of the oligomers present are "inert" trimers composed of two fibrinogen monomers and one fibrin monomer, the species we denote by  $C_{120}$ . Exploration of how variations in the fibrinogen binding rate y modulates the influence of fibrinogen binding on the polymerization system is shown in Figs. 14 and 15 in Appendix E. There, we show and explain the insensitivity of the border between no-gel and gel regions in the  $\eta_m$ - $\gamma$ parameter plane to variations in  $\nu$  for  $\nu > 2$ .

# B. Case 2: Monomeric conversion only $(\eta_o = 0)$

By allowing only monomeric fibrinogen to be converted to fibrin monomers, this limiting case where  $\eta_o \ \ \ \eta_m$  explores the dynamics of the system when fibrinogen can either inhibit gelation through fibrinogen binding or enhance gelation through monomeric conversion. We assume that only fibrinogen is present initially, so  $\varphi = 1$ , and all fibrin is supplied by conversion of monomeric fibrinogen. For these studies, we solve Eqs. (23)–(32) with  $\eta_m > 0$ ,  $\eta_o = 0$  and with initial conditions given by Eqs. (34) with  $\varphi = 1$ .

We first investigate how varying the monomeric conversion rate  $\eta_m$  affects gel time. Figure 6(a) shows the variation in  $\tau_{\rm gel}$  with  $\eta_m$  and  $\kappa$  for  $\gamma = 1$ . The solid black curve again partitions parameter space into gel and no-gel regions. For some values of  $\kappa$  in Fig. 6(a), there is a minimum  $\eta_m$  value necessary for a gel to form, while for higher values of  $\kappa$ , a gel forms for all  $\eta_m$  values considered; however,  $\tau_{\rm gel}$  is high for large  $\kappa$  and small  $\eta_m$ . An increase in  $\eta_m$  allows more fibrin to participate in branching reactions and reduces the pool of fibrinogen that can bind with oligomer, and inhibit further oligomer growth.

Recall that, in the current case, the binding of a fibrinogen monomer to an oligomer hinders gelation in two ways: (i)

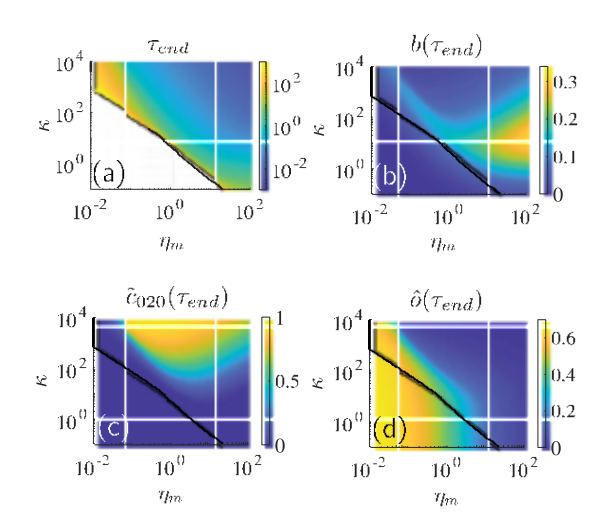


FIG. 6. (Case 2) For various monomeric conversion rate  $\eta_m$  and branching rate  $\kappa$  values with fibrinogen binding rate  $\nu = 1$ , heatmaps of (a)  $\tau_{\rm end}$  and concentrations at  $\tau_{\rm end}$  of (b) branches b, (c) fibrinogen monomer  $\tilde{c}_{020}$ , and (d) fibrinogen in oligomer  $\hat{o}$ . Black curves depict the gel/no-gel boundary.

by preventing that fibrinogen monomer from becoming fibrin; and (ii) by permanently blocking a fibrin reaction site on the oligomer. Therefore,  $\tau_{\rm gel}$  decreases as  $\eta_m$  increases; this is reminiscent of the result from Ref. [6], where faster supply of monomer leads to shorter gel times.

Figure 6 also shows heatmaps of the concentrations of branch points, fibrinogen monomer, and fibrinogen in oligomers at  $\tau_{\rm end}$  as functions of  $\eta_m$  and  $\kappa$  for  $\gamma = 1$ . The heatmap of branch concentration in Fig. 6(b) indicates that branch formation is strongly limited in the no-gel region and that the branch concentration varies nonmonotonically in  $\kappa$  for fixed  $\eta_m$  and is nonmonotonic in  $\eta_m$  for a sufficiently large fixed value of  $\kappa$ . The monomeric fibrinogen concentration at simulation's end in Fig. 6(c) also shows nonmonotonic behavior in  $\eta_m$  for large  $\kappa$  values.

A high concentration of fibrinogen monomer at simulation's end, shown in Fig. 6(c), exists only in parameter regions where a gel forms, and in particular, for large  $\kappa$ . Figure 6(a) shows that the gel time for the same parameter region is small, indicating that gelation occurs before much fibrinogen monomer can be incorporated into oligomers. In the no-gel region, no fibrinogen monomer remains at the end of simulation.

Complementary to these observations, the concentration of fibrinogen in oligomer is large in the no-gel regions as shown in Fig. 6(d). A large concentration is found almost exclusively in the no-gel region, with a high concentration of oligomeric fibrinogen in the gel region only for large  $\kappa$  and small  $\eta_m$ . Since Fig. 6(a) shows that gel times within that part of the gel region are large, the longer time allows for fibrinogen monomer to bind to other oligomers, resulting in a higher oligomeric fibrinogen concentration.

Figure 17 in the Appendix E shows how variations in the fibrinogen binding rate  $\gamma$  affect whether a gel forms, the time it forms, and the gel-time concentrations of fibrin reaction sites r, branches b, and fibrinogen monomer  $\tilde{c}_{020}$ .

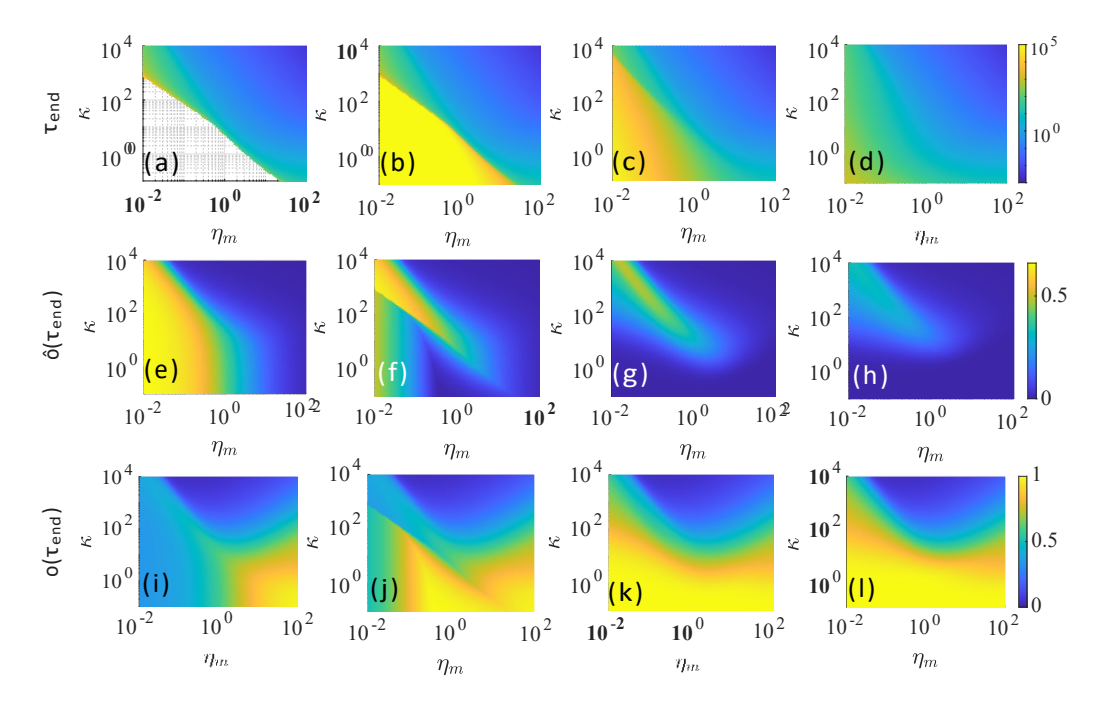


FIG. 7. (Cases 2 and 3) (Row 1)  $\tau_{\text{end}}$ , (Row 2)  $\hat{o}(\tau_{\text{end}})$ , and (Row 3)  $o(\tau_{\text{end}})$  as functions of branching rate  $\kappa$  and conversion rate  $\eta_m$ . Columns from left to right:  $\eta_o/\eta_m = 0$  (Case 2),  $10^{-5}$ ,  $10^{-1}$ , 1. Panel (a) shows the same data as Fig. 6(a) with a different colorbar range.

## C. Case 3: Monomeric and oligomeric conversion $(\eta_{\theta} > 0)$

To determine how oligomeric conversion of fibrinogen affects gel time and concentrations of interest, we allow oligomeric conversion to occur at a specified fraction of the monomeric fibrinogen conversion rate, that is, we vary  $\eta_o/\eta_m$  from zero to one. Figure 7 shows how the gel time  $\tau_{\rm gel}$  and concentrations of interest at the end of the simulation vary as functions of the branching rate  $\kappa$ , monomeric conversion rate  $\eta_m$ , and oligomeric conversion rate,  $\eta_o$ . The columns, from left to right, depict results for  $\eta_o/\eta_m = 0$ ,  $\eta_o/\eta_m = 10^{-5}$ ,  $\eta_o/\eta_m = 10^{-1}$ , and  $\eta_o/\eta_m = 1$ . For large  $\kappa$  and large monomeric conversion rate, corresponding to the upper right quadrant of each heat map, concentrations, and gel times are similar for all values of  $\eta_o$  considered, indicating ranges of parameter values for which Cases 2 and 3 exhibit similar behavior.

For low  $\kappa$  and low  $\eta_m$  values, varying  $\eta_o$  alters both the gel time and the structure of the clusters at gel time. For this  $\kappa$ and  $\eta_m$  region, Figs. 7(a)–7(d) show that  $\tau_{gel}$  decreases as the oligomeric conversion rate increases. Since  $\eta_m$  is small and therefore conversion of monomeric fibringen to fibrin is slow, changing  $\eta_o$  can significantly change the overall con-version rate. Furthermore, for these low  $\kappa$  values, free fibrin reaction sites are slowly incorporated into branches and thus are subject to binding by fibringen for long periods. Without oligomeric fibrinogen conversion to fibrin, this would result in permanent obstacles to further polymerization. With a low rate of oligomeric conversion, these obstacles are eventually removed, but the time until gelation is long. In fact, the gel times vary by more than seven orders of magnitude; the white space in Fig. 7(a) is a no-gel region and at points in the bright vellow region in Fig. 7(b),  $\tau_{gel} > 10^5$ .

The concentrations of fibrinogen in oligomer,  $\hat{o}$ , and fibrin in oligomer, o, are shown in Figs. 7(e)–7(h) and Figs. 7(i)–7(l),

respectively. Unsurprisingly, as  $\eta_o$  increases the concentration of fibrinogen in oligomer decreases, while the concentration of fibrin in oligomer increases. As  $\eta_o/\eta_m$  increases from 0 to 1, Figs. 7(e)–7(h) show that  $\hat{o}$  decreases throughout parameter space but does so more strongly, especially for lower  $\eta_o/\eta_m$  values, at points in the no-gel region of Fig. 7(a). As shown in Figs. 7(i)–7(l), fibrin in oligomer, o, increases with increasing  $\eta_o/\eta_m$ , again nonuniformly with the greatest change occurring in the no-gel region.

Figures 8(a) and 8(b) shows the concentration of branches at the end of the simulations for  $\eta_o/\eta_m = 0$ , as in Case 2, and for  $\eta_o/\eta_m = 1$ , and we see that the concentration is insensitive to the changes in  $\eta_o/\eta_m$ . To understand this insensitivity, we

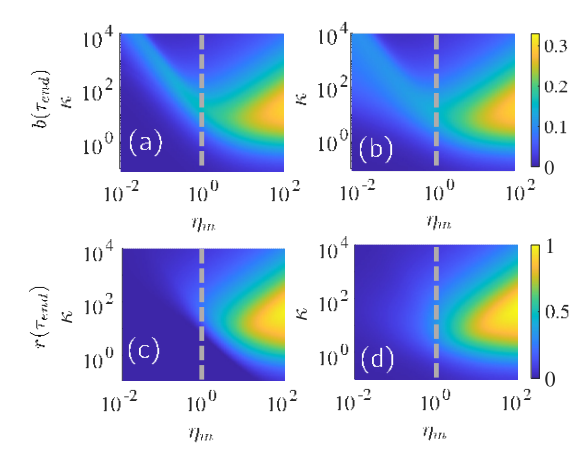


FIG. 8. (Case 2 and Case 3) For various monomeric conversion rate  $\eta_m$  and branching rate  $\kappa$  values, concentrations at  $\tau_{\rm end}$  of (a, b) branches b and (c, d) free fibrin reaction sites r. Left column shows results for Case 2 with  $\gamma = 1$  and  $\eta_o = 0$ . Right column shows results for  $\gamma = 1$  and  $\gamma$ 

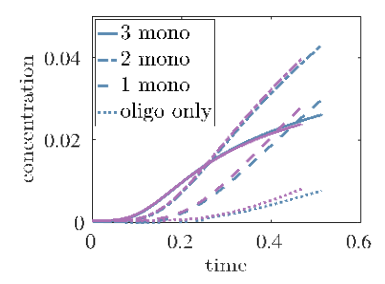


FIG. 9. (Case 3) Concentration of branches formed through reactions involving exactly three fibrin monomers (solid), exactly two fibrin monomer (dash-dotted), exactly one fibrin monomer (dashed), and oligomers only (dotted) for  $\gamma = 1$ ,  $\kappa = 100$ ,  $\eta_m = 1$ . The line colors denote  $\eta_o = 0$  (blue) and  $\eta_o = 1$  (purple).

calculate the total concentration of branches formed through the different branching reactions which involve different combinations of fibrin monomers and oligomers. The overall rate of branch formation  $\frac{\kappa}{6}r^3$  from Eq. (27) can be written as

$$\frac{\kappa}{6}r^{3} = \frac{4}{3}\kappa c_{102}^{3} + 2\kappa c_{102}^{2}(r - 2c_{102}) + \kappa c_{102}(r - 2c_{102})^{2} + \frac{\kappa}{6}(r - 2c_{102})^{3},$$
 (35)

where the terms on the right-hand side correspond to the *rates* at which branches form via reactions involving three fibrin monomers, two fibrin monomers and an oligomer, two oligomers and a fibrin monomer, and three oligomers, respectively.

The cumulative contribution to the concentration of branches made by each of the four processes can be calculated by integrating each term in that equation with respect to time. For  $\eta_o = \eta_m$ ,  $\kappa = 100$ , and  $\gamma = 1$ , Fig. 9 shows that the majority of branches are formed through reactions involving two or more fibrin monomers. Since oligomeric conversion of fibrinogen does not increase the amount of fibrin monomer available, increasing  $\eta_o$  has little effect on the branch concentration.

We compare the free reaction site concentrations in Figs. 8(c) and 8(d) and we focus on the points indicated by the gray line segment in each heatmap. The points on this line segment for  $\kappa < 10$  are in the no-gel region when  $\eta_0 = 0$ . In Fig. 8(c), with  $\eta_0 = 0$  the concentration of free reaction sites is very low for parameter values along this line segment (low  $\kappa$ and moderate  $\eta_m$ ). In contrast, they are moderately high for parameter values corresponding to points just above the middle of the line segment for the  $\eta_0 = \eta_m$  case shown in Fig. 8(d). The difference is seen more clearly in the graphs of  $r(\tau_{\rm gel})$  and  $b(\tau_{\rm gel})$  for points along the lower portion of the line segment shown in Fig. 16 in Appendix E. This behavior is consistent with results in Figs. 7(e)-7(h) which show that for these parameter values, the concentration of fibrinogen in oligomers decreases as  $\eta_o/\eta_m$  is increased. Recall that a  $C_{mgk}$ oligomer has g free fibrinogen reaction sites and k free fibrin reaction sites, and that the number of branches b is related to these as k = b + 2 - g. Decreases in g and increases in k are correlated if the branch number changes are small.

To look at the direct effect of fibrinogen binding, we compare a Case 3 simulation with  $\gamma = 1$  and  $\eta_o = \eta_m$  to a

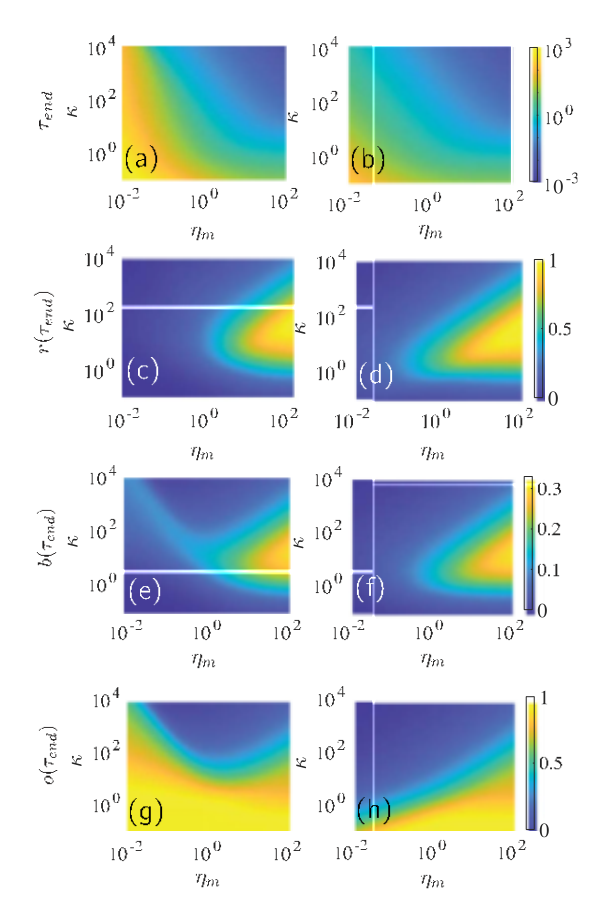


FIG. 10. (Case 3 and fibrin-only case) For various  $\eta_m$  and  $\kappa$  values, (a, b)  $\tau_{\rm end} = \tau_{\rm gel}$ , and concentrations at  $\tau_{\rm end} = \tau_{\rm gel}$  of (c, d) fibrin in oligomer, (e, f) branches, and (g, h) free reaction sites. Left column shows results for Case 3 with  $\gamma = 1$  and  $\eta_o = \eta_m$ . Right column shows results for  $\gamma = 0$ , corresponding to Fibrin-only polymerization. Panel (a) shows the same data as Fig. 7(d), with a different colorbar range and panel (e) shows the same data as in Fig. 8(b).

simulation with no fibrinogen binding with y = 0 [8] as we vary  $\kappa$  and  $\eta_m$ . Because oligomers in the case  $\gamma = 0$  consist only of fibrin, we refer to this as the "fibrin-only" Case. Figures 10(a) and 10(b) show that for both cases, a gel forms for all values of  $\kappa$  and  $\eta_m$  considered and that gel times vary by over five orders of magnitude as  $\kappa$  and  $\eta_m$  are varied. For any  $\kappa$ and  $\eta_m$ , gelation occurs later if fibrinogen binding is allowed, with the greatest delay occurring for small values of  $\eta_m$ . In Figs. 10(c) and 10(d), we see that the total concentrations of reactive sites r at  $\tau_{gel}$  are very similar in the two cases across all  $\kappa$  and  $\eta_m$  values considered. Figures 10(e)-10(h) show that for  $\eta_m > 1$ , the concentrations at  $\tau_{gel}$  of branches and of fibrin in oligomers are quite similar whether y = 0 or y = 1. In contrast, there are significant differences in both o and b for the two values of  $\gamma$  for  $\eta_m < 1$ : (i) the concentration of fibrin in oligomers is higher, by up to a factor of about 4 for a range of  $\kappa$ values when fibringen binding is allowed, and (ii) there is clear nonmonotonicity in the branch concentration when fibring is allowed, but not for the fibrin only case. More specifically, if fibringen binding is allowed, then there is a swath of parameter space running between the center

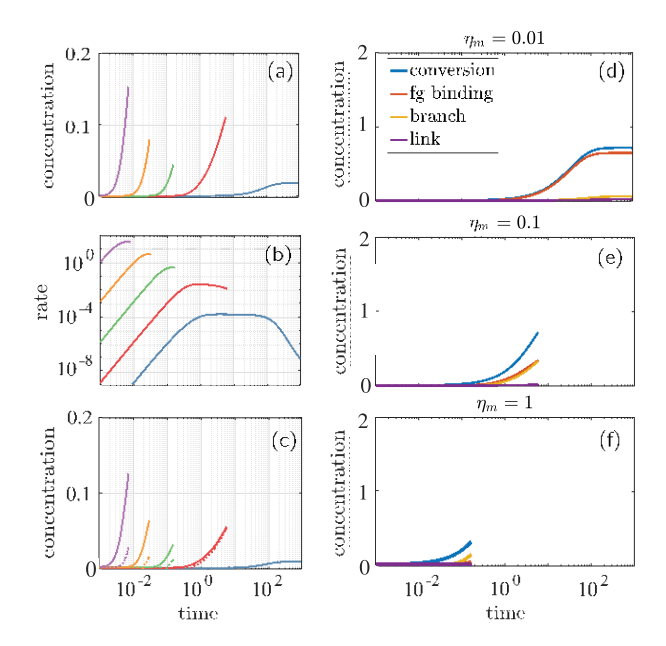


FIG. 11. (Case 2) Branch concentration, branch reaction rates, and cumulative production and consumption of free reaction sites for  $\gamma = 1$ ,  $\kappa = 10^3$  and varying conversion parameter  $\eta_m$ . Time courses of (a) branch concentration, (b) branch formation rate, and (c) concentrations of branches made in reactions involving (solid) two or more monomers or (dotted) two or more oligomers. Conversion rate  $\eta_m = 10^{-2}$  (blue),  $10^{-1}$  (red),  $10^0$  (green),  $10^1$  (orange),  $10^2$  (purple). Time courses (d, e, f) of the integral of the individual terms in Eq. (26), which are related to fibrinogen conversion, fibrinogen binding, branch formation, and link formation.

and the upper left corner of the heatmap in which the branch concentration is higher than in the adjacent regions on both sides of the swath.

To obtain more insight into the nonmonotonic behavior of  $b(\tau_{\rm gel})$  with respect to variations in  $\eta_m$ , as shown in Figs. 8(a) and 8(b) [and Fig. 10(e)], we plot  $b(\tau)$  for various  $\eta_m$  values in Fig. 11(a) with  $\eta_o = 0$  (Case 2). The right end point of each curve is  $[\tau_{\rm gel}, b(\tau_{\rm gel})]$  for the associated  $\eta_m$  value and these  $b(\tau_{\rm gel})$  values reprise the nonmonotonicity seen in Fig. 8(a). For each 10-fold decrease in  $\eta_m$ , there is an approximately 10-fold longer delay before the branch concentration noticeably begins to rise. There is then a period of accelerating branch formation.

Figure 11(b) shows that for  $\eta_m > 1$ , gelation occurs by  $\tau = O(10^{-1})$  and branch formation continues to accelerate until just before  $\tau_{\rm gel}$ . For  $\eta_m$  6  $10^{-1}$ , the branch formation rate reaches its peak value at about  $\tau = 1$  and then remains near that value for an extended period of time (note that  $\tau$  is plotted on a log scale). For  $\eta_m = 10^{-1}$ , branches form at near the peak rate until time  $\tau_{\rm gel} \approx 9$ ; for  $\eta_m = 10^{-2}$ , the branch formation rate remains near its peak until  $\tau \approx 100$ , before then dropping sharply (as fibrinogen is depleted-not shown) until a gel forms at  $\tau_{\rm gel} \approx 10^3$ . While the peak rate for  $\eta_m = 10^{-1}$  is about 20-fold lower than for  $\eta_m = 1$ , branch formation at near the peak rate continues for a much longer time and this results in a higher value of  $b(\tau_{\rm gel})$ . When  $\eta_m$  changes from  $10^{-1}$  to  $10^{-2}$ , the reduction in peak branching rate is not compensated for by the extended duration of near

peak rate branch formation and this leads to lower cumulative branch formation for  $\eta_m = 10^{-2}$ .

Recall that nonmonotonicity is not seen in the fibrin-only simulations ( $\gamma = 0$ ) shown in Fig. 10(f), and that the gel times when  $\gamma = 1$  are much longer than the corresponding ones when  $\gamma = 0$  [compare Figs. 10(a) and 10(b)]. The behavior of the model depends on the production and use of fibrin reaction sites. To examine the role of fibrinogen binding with  $\gamma = 1$  in the nonmonotonicity, we looked at the cumulative production of reaction sites up to time  $\tau$  by conversion of fibrinogen and the cumulative consumption of reaction sites up to that time by each of link formation, branch formation, and fibrinogen binding. These quantities, which are, respectively, the integral up to time  $\tau$  of  $2\eta_m\tilde{c}_{020}$ ,  $r^2$ ,  $\frac{3\kappa}{2}r^3$ , and  $2\gamma\tilde{c}_{020}r$  [see Eq. (26)] are shown in Figs. 11(d)–11(f) for  $\eta_m = 1$ , 0.1, and 0.01 corresponding to the green, red, and blue curves, respectively, in Figs. 11(a) and 11(b).

Looking at the production curves, we see that for each  $\tau$ for which multiple such curves are defined, production was greater for higher  $\eta_m$ . However, the cumulative production of reaction sites by  $\tau_{gel}$  increased as the conversion rate  $\eta_m$  decreased. A maximum cumulative production of 2 is possible; the actual cumulative production up to gel time was  $\approx 0.32$ ,  $\approx 0.72$ , and  $\approx 0.71$  for  $\eta_m = 1$ , 0.1, and 0.01, respectively. Cumulative production is still increasing rapidly at  $\tau_{gel}$  for the two larger values of  $\eta_m$ , but has plateaued for  $\eta_m = 0.01$ indicating depletion of fibrinogen. We see that for all three values of  $\eta_m$ , link formation consumed only a small portion of the reaction sites. For  $\eta_m = 1$ , most of the reaction sites produced were still present at gel time, with branch formation consuming more reaction sites than fibringen binding or link formation. For  $\eta_m = 0.1$ , a much smaller fraction of the reaction sites produced were present at gel time, and consumption by branch formation was approximately equal to that by fibrinogen binding. So, for  $\eta_m = 0.1$ , not only were reaction sites produced more slowly, but also close to half of the sites produced were blocked by fibrinogen binding. For  $\eta_m = 0.01$ , until  $t \approx 10$ , fibringen binding consumed almost all of the reaction sites produced. After this time, fibrinogen binding slowed dramatically because of fibrinogen depletion, allowing the remaining reaction sites to be utilized primarily for branch formation.

We see that the conversion rate  $\eta_m$  influences not only how fast fibrin monomers are produced, but also the use to which fibrin reaction sites are put, with a much larger fraction being blocked by fibrinogen binding for  $\eta_m = 0.01$ , balanced consumption to form branches and by fibrinogen binding for  $\eta_m = 0.1$ , and more used for branch formation for  $\eta_m = 1$ . There are two pairs of rate comparisons which seem to be key: (i) the rate of producing reaction sites by the conversion of fibringen monomers into fibrin  $2\eta_m \tilde{c}_{020}$  compared with the rate of binding of fibringen to fibrin reaction sites  $2\gamma r\tilde{c}_{020}$ and (ii) the rate that reaction sites are used to form branches  $\underline{\kappa}$  $r^3$  compared to the rate they are used to bind fibringen  $2\gamma \tilde{c}_{020}r$ . For the first, the issue is which of  $\eta_m$  and  $\gamma r$  is larger, and for the second, the issue is which of  $\underline{\kappa}^2$  and  $2\gamma \tilde{c}_{020}$  is larger. In both comparisons, the prescribed values of the parameters  $\eta_m$ ,  $\gamma$ , and  $\kappa$  matter, but so does the current reaction site concentration r. If  $\eta_m > \gamma r$  and  $\frac{\kappa}{2}r^2 > 2\gamma \tilde{c}_{020}$ , then both conversion of fibrinogen and branch formation dominate

fibrinogen binding. Both inequalities hold if r satisfies

$$\frac{^{3}}{\kappa} \frac{4\gamma \,\tilde{c}_{020}}{\kappa}^{^{1/2}} < r < \frac{\eta_{m}}{\gamma}. \tag{36}$$

The upper bound is fixed once parameters are chosen, and from Eq. (26) with  $\eta_o = 0$  since we are discussing Case 2, we see that if r(0) = 0, then  $2\gamma r(\tau)\tilde{c}_{020}(\tau)$  6  $2\eta_m\tilde{c}_{020}(\tau)$  for all  $\tau$ > 0. Hence, the second inequality in Eq. (36) is always satisfied. However, the lower bound decreases as fibrinogen monomer is consumed and  $\tilde{c}_{020}$  decreases. A large value of  $\eta_m$ leads to fast increases in r and fast decreases in  $\tilde{c}_{020}$ , making the left inequality easier to satisfy and allowing branch formation to dominate. A low value of  $\eta_m$  leads to slow growth in r both because fibringen is converted more slowly and because fibringen binding to the fibrin that is produced is relatively rapid. While r is small, branching occurs at a relatively slow rate, thus delaying or preventing gelation. Further results about and discussion of the changes in relative timescales as  $\eta_m$ ,  $\kappa$ , and  $\gamma$  are varied is presented in Figs. 18–22 and the text surrounding them in Appendix E.

Related to the availability of fibrin monomers is the type of branch forming reactions that dominate for different values of  $\eta_m$ . As shown in Fig. 11(c), branch formation reactions involving two or more monomers dominate for  $\eta_m > 1$ , but production of branches through reactions that use one or no monomers, i.e., those involving mostly oligomers, is about equal to these for  $\eta_m = 0.1$  and is dominant for  $\eta_m = 0.01$ .

### D. Oligomer functionality and stochastic simulations

Kinetic gelation models with fixed monomer functionality require the functionality to be greater than two for gelation to be possible and reactions in these models are assumed to be bimolecular [13]. Here, we assume that both fibrin and fibringen monomers have a fixed functionality of two, but higher functionality is achieved through the trimolecular branch reaction. Fixed monomer functionality of two has also been assumed in our previous fibrin-only models of polymerization [6,8]. A key metric in Ref. [8] is the number-average number of functional sites per cluster, or number-average functionality, and is defined as the ratio of the concentration of free (fibrin) reaction sites to the concentration of clusters of all sizes. In the notation of the current paper this would be expressed  $f_A = r/m_{000}$ . It is a dynamic quantity that, for that model, is greater than 2 whenever gelation occurs. For the present study, this definition is inappropriate. As a result of fibringen binding, there may be many clusters which have no free fibrin reaction sites at all, and these "inert" clusters cannot participate in any binding reactions. Clusters with exactly one free reaction site may also be numerous and these clusters participate only in reactions in which the functionality of the product is less than that of the reactant with the greater functionality. A measure of number-average functionality potentially more appropriate for the current situation is computed by dividing the total concentration of free fibrin sites, counting only clusters with at least two such sites, by the total concentration of clusters with at least two reaction sites. We call this metric  $f_A^{(2)}$ , and we define  $f_A^{(1)}$  similarly based on clusters with at least one reaction site. We hypothesize that gelation occurs in the current model only when  $f_A^{(2)} > 2$  in the

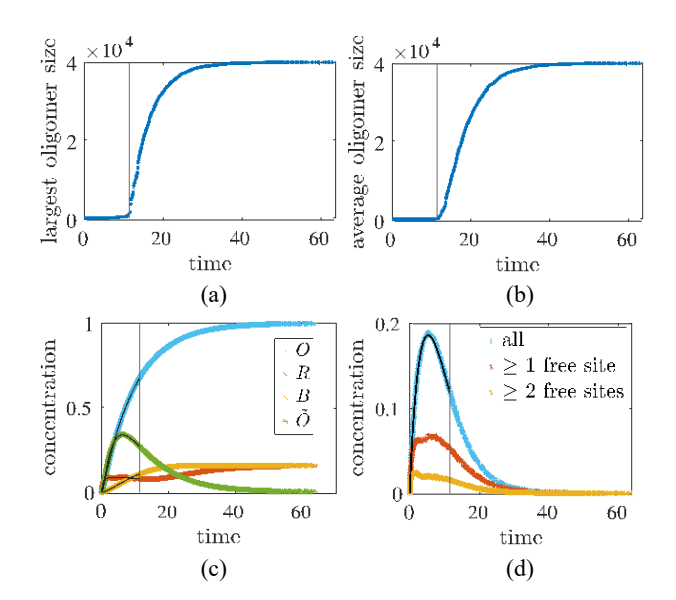


FIG. 12. (Gillespie simulations) Rate constants  $\kappa = 100$ ,  $\gamma = 1$ ,  $\eta_m = 0.1$ ,  $\eta_o = 0.1$  for Case 3. Number of monomers  $N = 4 \times 10^4$ . (a) Largest oligomer vs time, (b) weight-average oligomer size vs time, (c) deterministic (black) and stochastic concentrations of fibrin in oligomer (blue), free reaction site (red), branch (yellow), and fibrinogen in oligomer (green) vs time, and (d) concentration of all clusters,  $M_{000}$  (blue), clusters with at least one free reaction site (red), and at least two free reactions sites (yellow).

time leading up to gelation. However, information about these subpopulations of oligomers is not available from the solutions of Eqs. (23)–(32), although it would be from the solution of the system Eqs. (12)–(13) from which these equations were derived.

To investigate the number-average functionality of noninert species, we used the Gillespie method [29,30] to stochastically simulate the reactions (see Appendix D) whose deterministic description is Eqs. (12)–(13). Within the stochastic simulations, it is straightforward to track the subpopulations of oligomers with no free reaction sites, those with exactly one such site, and those with two or more sites. In the stochastic simulations, there is a finite number of monomers, so the weight-average oligomer size cannot "blow-up." However, the size of the largest oligomer and the weight-average oligomer size begin to sharply increase starting at the gel time predicted by the deterministic ODE system (vertical line), as shown in Figs. 12(a) and 12(b). Figure 12(c) shows plots of o, r, b, and  $\hat{o}$ from the Gillespie simulations (color) and the deterministic ODE system Eqs. (23)-(32) (black). We see excellent agreement between the stochastic and deterministic concentrations for  $\tau$  6  $\tau_{gel}$ ; thus, we can use the stochastic simulation to further assess the polymerization system. Figure 12(d) shows how the concentrations of all clusters,  $M_{000}(t)$ , clusters with at least one free reaction site, and clusters with at least two free reaction site depend on time. As expected, the concentration of clusters with at least one free reaction site is much smaller than the concentration of all clusters, indicating that many clusters have no available free sites and are inert species. We also see that for much of the simulation, there are many oligomers with exactly one reaction site.

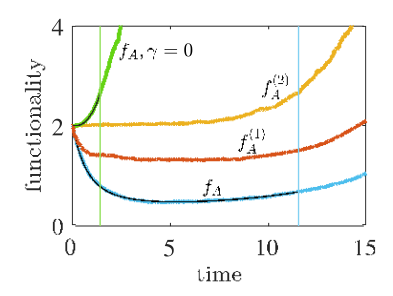


FIG. 13. (Case 3) Number-average functionality vs time from deterministic (black) and stochastic [29,30] simulations (color). The green curve shows the number-average functionality,  $R/M_{000}$  in the fibrin-only case (green), where  $\gamma = 0$ ,  $\eta_m = 0.1$ ,  $\kappa = 100$ . For the other curves,  $\gamma = 1$ ,  $\gamma_0 = \gamma_m = 0.1$ ,  $\kappa = 100$ . Number-average functionality in stochastic simulations is shown for all oligomers  $f_A$  (blue), for oligomers with at least one free reaction site  $f_A^{(1)}$  (red), and for oligomers with at least two free reaction sites  $f_A^{(2)}$  (yellow). Vertical lines denote gel times found by solving the ODE system Eqs. (23)–(32) until  $\nu \to 0$ .

We carried out stochastic simulations with conversion rates  $\eta_m = \eta_o = 1$ , branching rate  $\kappa = 100$ , and fibrinogen binding rate y = 1 for the fibrinogen-fibrin system and, by setting y = 0, for the fibrin-only system. To compare results from the full system with those from the fibrin-only simulation, we par-tition the clusters contributing to  $m_{000}$  into subpopulations of clusters with no free reaction sites, one or more free reaction sites, or two or more free reaction sites and we compute the quantities  $f_A$ ,  $f_A^{(1)}$ , and  $f^{(2)}$  described above. Figure 13 shows the concentration  $f_A = r/m_{000}$  from the deterministic system (black) and the stochastic simulations (color). We compare  $f_A$  from the fibrin-only simulation (green) with  $f_A$ ,  $f_A^{(1)}$ , and  $f_A^{(2)}$ from the fibrinogen-fibrin simulation, shown in blue, red, and yellow, respectively. The number-average functionality  $f_A$  for the fibrin-only system increases monotonically in time and is above 2 at gel time, while the number-average functionality for the fibrin-fibrinogen model including all clusters is much lower than 2. However, the number-average functionality  $f_A^{(2)}$ of clusters with at least two free sites is larger than 2 at gel time and is comparable to the number-average functionality of the fibrin-only clusters at the fibrin-only gel time.

# IV. DISCUSSION

We have proposed a model of fibrin polymerization with fibrinogen interactions that includes mechanisms for fibrin branch formation, for fibrinogen binding to fibrin, and for fibrinogen in both monomeric and oligomeric form to be converted to fibrin. These reactions are combined into a kinetic polymerization model that is expressed in terms of an infinite set of oligomer concentrations,  $c_{mgk}$ . Each oligomer is defined by the number of free fibrin binding sites and the number of each type of monomer (fibrin and fibrinogen) contained in the oligomer. Using a moment generating function approach [6,13,28], we obtain a closed system of low-order moment equations that describe the dynamics of quantities of interest, up to gel time.

To our knowledge, this is the first mathematical model of fibrin polymerization up to gelation that incorporates fibrinogen's ability to be a source of fibrin and to bind to fibrin with a proposed mechanism for branching. These reactions allow us to determine how the inhibitory role of fibrinogen can affect the time to form a gel and the resulting gel structure. To fully understand our proposed model, our results are divided into three cases that are distinguished by which conversion reactions are allowed to occur.

Case 1 allows no conversion reactions and defines an initial composition parameter,  $\varphi$ , which specifies the fraction of fibrinogen in the initial mixture of fibrinogen and fibrin monomers. We explored how fibrinogen binding to fibrin reaction sites hinders gelation. We demonstrated that for a given branching rate  $\kappa$ , there exists a maximal value  $\varphi$  for which gelation can occur. This case is similar to a general model of two monomer polymerization [28]. In that study, each type of monomer had a prescribed functionality (number of binding sites), and as in Case 1 here, the initial mixture of monomers and the types of reactions allowed were varied. The gel time in Ref. [28] depended on the initial composition, the relative reaction rates, and the monomers' functionalities.

In the current paper, monomers have a fixed functionality of 2; it is only through branch formation that molecules of sufficiently high functionality appear so that gelation can occur. We allow for conversion of monomeric fibrinogen in Case 2 and assume that initially only fibrinogen is present, so that  $\varphi = 1$ . With both monomeric conversion and fibrinogen binding allowed, we examine how the dual role of fibrinogen, both hindering and facilitating gelation, can affect gel structure and gel time. Again, we show that there exists a gelation threshold; if both monomeric conversion and branching rates are sufficiently small (compared to the rate of fibrinogen binding to fibrin), fibrinogen binds to a large fraction of the available binding sites on the fibrin molecules and in so doing, prevents gelation.

For a very low monomeric conversion rate, gelation still occurs for a sufficiently large branching rate  $\kappa$ , but it takes a long time for a gel to appear. In this situation, conversion of fibringen monomers to fibrin is the rate-limiting step and the gel time reaches as high as  $O(10^3)$ , almost four orders of magnitude larger than the gel time when the monomeric conversion rate is high. Polymerization occurs slowly and during the long period of time until a gel is formed, more fibringen is incorporated into the gel and more branches are formed. Allowing for both oligomeric and monomeric conversion at the same rate in Case 3, the system gels for all parameter values but can exhibit large gel times in parameter regimes where the conversion and branching rates are small. For all  $\kappa$ and  $\eta_m$  values considered, the concentrations of b and r are similar for  $\eta_o/\eta_m$  values of 0,  $10^{-5}$ ,  $10^{-1}$ , and 1, where  $\eta_o$  is the rate at which oligomer-bound fibrinogen is converted to fibrin. For large  $\kappa$  and  $\eta_m$  values, the fibrin in oligomer and the fibrinogen in oligomer concentrations are similar for these values of  $\eta_o/\eta_m$ .

Branch formation, a trimolecular reaction, can be characterized by how many monomers are involved in the reaction. We examine how the rate of each of the four types of branch formation reaction changes as  $\eta_m$  and  $\eta_o$  are varied. For most parameter values, more branches are formed through reactions that involve at least two monomers, but for sufficiently low  $\eta_m$  values, reactions that involve mostly oligomers are the

dominant form of branch formation. This switch in the dominant branch forming mechanism is similar to that seen in a model of fibrin branching with a constant source of fibrin monomer as the branching rate was varied [6], but here the switch is related more to the relative rates of monomer conversion, fibrinogen binding and branch formation.

For large conversion rates, the branch concentration at gel time increases as  $\eta_m = \eta_o$  increases; this is seen biologically, where branch number at gel time increases with thrombin [3], thus leading to "fine" clot with high density of branch points. A quasi-steady-state analysis of our earlier model with no fibrinogen binding and with a constant fibrin source rate can explain the nonmonotonic behavior for varying branching rate in that model, as a crossover between different scaling behaviors seen for very small and very large branching rates [8]. The fibrin-only model does not exhibit nonmonotonicity with changes in  $\eta_m$ . With fibrinogen binding allowed, the nonmonotonicity with respect to variations in  $\eta_m$  is a result of competition in how fibringen monomers are used—for fibrin formation or to block fibrin reaction sites—and competition of how fibrin reaction sites are used—being blocked by fibrinogen or participating in branch formation. The value of  $\eta_m$ directly affects the first competition, and indirectly affects the second competition by influencing the value of the reaction site and fibrinogen monomer concentrations.

Because values of critical parameters, in particular the branching rate  $\kappa$ , are unknown, we have not attempted to quantitatively compare our results with experiments. Our results are qualitatively similar to experimental results. We see that increasing  $\eta_m$  over ranges of several orders of magnitude results in gel times that decrease by several orders of magnitude. If we think of varying  $\eta_m$  as representing varying concentrations of thrombin, then our results agree with the behavior of gel times seen experimentally [1]. In the same study, branch concentration was seen to increase substantially as thrombin increased. For a range of  $\kappa$  values, we also see a large increase in branch point density as  $\eta_m$  is increased from  $10^{-2}$  to  $10^2$ . Other experiments show that for very small thrombin concentrations, virtually all oligomers contain bound fibrinogen [12]. We see a high concentration of oligomer-bound fibringen for small  $\eta_m$  in both Cases 2 and 3.

Fibrin polymerization is only one component of the blood clotting process. We have not discussed how spatial-temporal heterogeneities in thrombin concentration (and consequently in the rate of fibringen conversion) form under flow, and how the presence of other species, such as platelets, affects the formation of the gel structure. When formed under flow conditions, fibrin fibers align with the flow field and fiber thickness decreases as shear rate increases [31,32]. Additionally, thrombin is produced on the surface of activated platelets through a system with strong positive feedback mechanisms and this results in a localized burst in the thrombin concentration [33]. These all contribute to the development of a heterogenous fibrin clot structure that is more diffi-cult to degrade by fibrinolysis compared to clots formed without platelets [33,34]. Understanding how thrombin heterogeneities and flow impact the availability of fibrinogen to bind and aid in fibrin gel formation is a subject of further investigation.

#### ACKNOWLEDGMENTS

This work was supported in part by National Science Foundation Grant No. DMS-1716898 and NHLBI Grant No. R01HL151984 to A.L.F. A.C.N. was partially supported by National Science Foundation Grants No. DMS-1716898 and No. DMS-2038056, as well as a scholarship from BioFire Diagnostics.

#### APPENDIX A: DERIVATION OF MOMENT EQUATIONS

To derive low-order moment equations, we use Eqs. (16) and (17). For example, setting x = y = z = 1 in Eq. (16), we obtain

$$\frac{dM_{000}}{dt} = -\frac{k_l}{2}R^2 - \frac{k_b}{3}R^3 + k_m c_{020}.$$
 (A1)

Differentiating each term in Eq. (16) with respect to only x, only y, and only z, respectively, and setting x = y = z = 1, we obtain

$$\frac{dM_{100}}{dt} = -\frac{k_b}{3}R^3 + k_m c_{020} + k_o M_{010},\tag{A2}$$

$$\frac{dM_{010}}{dt} = 2k_g c_{020} R - k_o M_{010},\tag{A3}$$

$$\frac{dR}{dt} = -k_1 R^2 - \frac{k_b}{2} R^3 - 2k_g c_{020} R + 2k_m c_{020} + k_o M_{010}.$$
(A4)

Similarly, we can show that

$$\frac{dM_T}{dt} = \frac{X}{m_{,g,k}} (m + 2g + 2k - 4) \frac{dc_{mgk}}{dt} = k_m c_{020} + k_o M_{010},$$
(A5)

$$\frac{d\hat{M}_T}{dt} = \frac{X}{m_{,g,k}} g \frac{dc_{mgk}}{dt} + \frac{dc_{020}}{dt} = -k_m c_{020} - k_o M_{010}.$$
 (A6)

Note that it then follows that

$$\frac{d}{dt}(M_T + \hat{M}_T) = 0, (A7)$$

and so the total concentration of fibrin and fibrinogen monomers is conserved, as it must be because monomer is neither created nor destroyed. The total concentration of fibrin in oligomers is  $O = M_T - c_{102}$  and similarly the total concentration of fibrinogen in oligomers is  $O = M_T - c_{020} = M_{010}$ . It then follows that

$$\frac{dO}{dt} = 2k_l c_{102}R + k_b c_{102}R^2 + 4k_g c_{102}c_{020} + k_o\hat{O}, \quad (A8)$$

$$\frac{d\hat{O}}{dt} = 2k_g c_{020} R - k_o \hat{O}. \tag{A9}$$

From the formula defining B in Eq. (20), we see that

$$\frac{dB}{dt} = \frac{X}{(k + g - 2)} \frac{dc_{mgk}}{dt} = k_b \frac{R^3}{6}.$$
 (A10)

For our analysis, we also need ODEs for the six second moments, i.e., the terms  $M_{abc}$  in Eq. (17) for which a + b + c = 2. It is straightforward to show that

$$\frac{dM_{200}}{dt} = k_l M_{101}^2 + k_b i R^3 - 2R^2 M_{101} + M_{101}^2 R^{\c} + 2k_o M_{110}, \tag{A11}$$

$$\frac{dM_{110}}{dt} = k_l M_{101} M_{011} + k_b (M_{101} M_{011} R - R^2 M_{011}) + 2k_g c_{020} M_{101} + k_o (M_{020} - M_{110}), \tag{A12}$$

$$\frac{dM_{101}}{dt} = k_l (M_{002} - R) M_{101} - 2k_g c_{020} M_{101} + k_b M_{101} M_{002} R - \frac{1}{2} R^2 M_{101} - R^2 M_{002} + 2k_m c_{020} + k_o (M_{010} + M_{110} + M_{011}), \tag{A13}$$

$$\frac{dM_{020}}{dt} = k_l M_{011}^2 + k_b M_{011}^2 R + 4k_g c_{020} M_{011} - 2k_o M_{020}, \tag{A14}$$

$$\frac{dM_{011}}{dt} = k_l (M_{002} - R) M_{011} + 2k_g c_{020} (M_{002} - M_{011}) + k_b R M_{011} M_{002} - \frac{1}{2} M_{011} R^2 + k_o (M_{020} - M_{011}), \tag{A15}$$

## APPENDIX B: BOUNDEDNESS OF $M_{002}$

 $-4k_{g}c_{020}M_{002} + 2k_{m}c_{020} + 2k_{o}M_{011}.$ 

Recall that gelation is defined as the occurrence of a finite time blow-up in the weight-average oligomer size A(t) which, if it occurs, happens at a time we denote  $t_{\rm gel}$ . We wish to show that  $A \to \infty$  if and only if  $M_{002} \to \infty$ . From Eq. (22), we see that A is a linear combination of all of the moments through second order divided by the (constant) total monomer concentration  $M_T + M_T$ . It is clear from the definition of A(t) and the boundedness of the first moments (see below) in its definition, that  $A(t) \to \infty$  if  $M_{002} \to \infty$ . We show below that if  $A(t) \to \infty$  then  $M_{002} \to \infty$ . Since  $M_{002}(t)$  blows up if and only if A(t) blows up, we can use the blow-up of  $M_{002}$  as an indicator that a gel has formed. We note that once this equivalence is established, we no longer need to compute the second moments  $M_{200}$ ,  $M_{101}$ , and  $M_{110}$  because they are not needed to evolve the physical concentrations or  $M_{002}$ .

To establish the boundedness claim, we examine the system of equations (A1)–(A16). First, consider the closed subsystem composed of Eqs. (13), (A3), (A4) for  $c_{020}$ ,  $M_{010}$ , and  $R = M_{001}$ , respectively. We assume that initially these variables are nonnegative. Then Eqs. (13), (A3), and (A4) imply that  $c_{020}$ ,  $M_{010}$ , and R remain nonnegative. Additionally, Eq. (13) implies that  $c_{020}$  is bounded for all t > 0. Adding Eqs. (13) and (A3) gives us  $\frac{d}{dt}(c_{020} + M_{010}) = -k_m c_{020} - k_o M_{010}$ , which implies that  $c_{020} = \frac{dt}{dt} M_{010} = \frac{d$ 

its right-hand side of Eq. (A2) are bounded. In summary, all first moments are bounded.

Consider Eqs. (A11)–(A16). Suppose  $M_{002}$  is bounded. Then by the form of Eq. (A16),  $M_{011}$  must also be bounded. Since Eq. (A14) is linear in  $M_{020}$  and all terms on the right-hand side are bounded,  $M_{020}$  is also bounded. The coupled equations (A12)–(A13) for  $M_{110}$  and  $M_{101}$  are linear with coefficients that are bounded. Hence, both  $M_{110}$  and  $M_{101}$  are bounded, and by Eq. (A11),  $M_{200}$  is also bounded. In summary, if  $M_{002}$  is bounded, then so are all of the other moments whose linear combination defines A, and so A is bounded.

#### APPENDIX C: RICCATI TRANSFORMATION

To simplify the discussion on boundedness of  $M_{002}$ , we define a new variable  $X = M_{002} - R$  and find that it satisfies

$$\frac{dX}{dt} = (k_l + k_b R)X^2 + (k_b R^2 - 4k_g c_{020})X$$
(C1)

+ 
$$k_b \frac{R^3}{2} - 2k_g c_{020} R + k_o (2M_{011} - \hat{O})$$
. (C2)

Since R remains bounded, X becoming unbounded at finite time is also an indication that gelation occurs at that time. The differential equation for X is a Riccati equation and takes the form

$$\frac{dX}{dt} = c(t) + b(t)X + a(t)X^{2}, \tag{C3}$$

where  $c(t) = k_b \frac{R^3}{2} - 2k_g c_{020}R + k_o (2M_{011} - O)$ ,  $b(t) = k_b R^2 - 4k_g c_{020}$ , and  $a(t) = k_l + k_b R$ . Therefore, by introducing a new variable V such that  $X = -\frac{dV}{dt}V$ , we can rewrite Eq. (C2) as a linear second order ODE of the form

$$\frac{d^2V}{dt^2} = -\frac{k_b}{2}R^3 - 2k_gc_{020}R + k_o(2M_{011} - O) aV \text{ (C4)}$$

$$+ k_bR^2 - 4k_gc_{020} + \frac{a^c}{a}\frac{\P}{dt}. \text{ (C5)}$$

Using these changes of variables in Eq. (A15) yields

$$\frac{dM_{011}}{dt} = k_l X M_{011} + k_b X + \frac{1}{2} R R M_{011} + 2k_g c_{020} (X - M_{011} + R) + k_o (M_{020} - M_{011}).$$
(C6)

Since  $V \to 0$  whenever  $X \to \infty$ , we now use  $V \to 0$  as a more convenient indicator of gelation. Finally, we nondimensionalize the equations by scaling all concentrations by the total initial concentration of monomers,

$$C_0 = c_{102}(0) + c_{020}(0),$$

and use  $\tilde{c}_{mgk}$  to denote the nondimensional concentration of oligomer  $C_{mgk}$  and lower case letters for the nondimensional moment concentrations and indicator function V. We scale time as  $\tau = k_l C_0 t$ . Four nondimensional parameter groups appear in the resulting nondimensional equations: branching rate  $\kappa = \frac{k_b C_0}{k_l^2}$ , fibrinogen-fibrin binding rate  $\gamma = \frac{k_g}{k_l^2}$ , monomeric fibrinogen conversion rate  $\eta_m = \frac{k_m}{k_l^2 C_0}$  and oligomeric fibrinogen conversion rate  $\eta_o = \frac{k^o}{k_l^2 C_0}$ . Defining  $\alpha = 1 + \kappa r$ , and

(A16)

using the nondimensional Riccati transformation  $x = m_{002} - r = -\frac{dv}{dt}/\alpha v$ , we obtain the closed system of nondimensional equations Eqs. (23)–(32). We also solve Eq. (12) in the instances (m, g, k) = (1,0,2), (1,1,1), and (1,2,0) to determine the concentrations of fibrin monomers  $\tilde{c}_{102}$ , fibrin-fibrinogen dimers  $\tilde{c}_{111}$ , and inert trimers  $\tilde{c}_{120}$ .

#### APPENDIX D: GILLESPIE IMPLEMENTATION

To further examine the dynamics of the polymerization system described in Sec. II, we performed stochastic simulations using the Gillespie Algorithm [29,30] in a volume v with N fibrinogen monomers  $C_{020}$  present initially. We denote the number of  $C_{m,g,k}$  monomers as  $n_{m,g,k}$ . Oligomers can participate in polymerization reactions or conversion reactions.

Oligomers  $C_{m_1g_1k_1}$  and  $C_{m_2g_2k_2}$  form a link during an infinitesimal time interval,  $\delta t$ , with probability  $v^{-1}k_1k_1k_2n_{m_1g_1k_1}n_{m_2g_2k_2}\delta t$  if  $(m_1,g_1,k_1)$  and  $(m_2,g_2,k_2)$  are distinct, and with probability  $(2v)^{-1}k_1k_2^2n_{m_2g_2k_2}(n_{m_2g_1k_1}-1)\delta t$  if  $(m_1,g_1,k_1)$  and  $(m_2,g_2,k_2)$  are the same. Oligomer  $C_{m_1g_1k_1}$  and fibrinogen monomer  $C_{020}$  bind together with probability  $v_{-1}k_gk_1n_{m_1g_1k_1}n_{020}\delta t$ .

A branch is formed by oligomers  $C_{m,g,k_1}$ ,  $C_{m,g,k_2}$ , and  $C_{m,g,k_3}$  with probability  $v^{-2}k_bk_1k_2k_3n_{m,g,k_1}n_{m,g,k_2}n_{m,g,k_3}\delta t$  if  $(m_1,g_1,k_1)$   $(m_2,g_2,k_2)$ ,  $(m_3,g_3,k_3)$  are all distinct. If  $(m_1,g_1,k_1)$  and  $(m_2,g_2,k_2)$  are the same but different from  $(m_3,g_3,k_3)$ , then the probability is  $v_1-k_bk_2k_3n_{m,g,k_3}k_3$ , then the probability is  $v_1-k_bk_3n_{m,g,k_3}k_3$ . If  $(m_1,g_1,k_1)(\bar{m}_2,g_2,k_2)$  and  $(m_1,g_1,k_1)$  are 3the same, then the probability of branch formation  $v_1-k_3k_3k_3$  is  $v_1-k_3k_3k_3n_{m,g,k_3}k_3$ . Finally, fibrinoger monomer  $v_1-k_3k_3n_{m,g,k_3}k_3$  is converted to  $v_1-k_3k_3n_{m,g,k_3}k_3$ , with probability  $v_1-k_3k_3n_{m,g,k_3}k_3$ , and oligomer  $v_1-k_3k_3n_{m,g,k_3}k_3$ , is converted to  $v_1-k_3k_3n_{m,g,k_3}k_3$ , with probability  $v_1-k_3k_3n_{m,g,k_3}k_3$ , and  $v_$ 

### APPENDIX E: SUPPLEMENTARY FIGURES

## 1. Case 1: Effects of $\gamma$ variations

We look at the behavior of the model Eqs. (23)–(32) in Case 1 (no conversion of fibrinogen to fibrin) for a range of fibringen binding rates  $\gamma$  and initial composition values  $\varphi$ . For these simulations, Fig. 14 indicates whether a gel forms, the time at which it forms, and the concentrations at simulation's end of branches, fibrinogen monomers, and fibringen in oligomers. The heat map in Fig. 14(a) shows the variation in  $\tau_{\rm gel}$ ; the white region indicates that a gel did not form for the corresponding parameter values. The black curves in each of the panels is the boundary between the gel and no-gel regions. We see that for large  $\gamma$  values, the no-gel region extends to lower  $\varphi$  values, indicating that more fibrin is required for gelation. For  $\nu \approx 2$  and above, the gel/no-gel boundary appears to be independent of  $\gamma$ . (An explanation for this behavior is given below.) Further we see that within the gel region,  $\tau_{gel}$  shows little sensitivity to  $\gamma$  for  $\gamma > 2$ .

Figure 14(b) shows that the branch concentration is larger when  $\tau_{\rm gel}$  is small and that few branches form in the no-gel region. The branch concentration varies strongly with  $\varphi$  and relatively weakly with  $\gamma$ ; the largest concentration of branches at gel time occurs when  $\varphi = 0$ , that is, when initially there are only fibrin monomers. The concentration of fibrinogen monomer,  $\tilde{c}_{020}$ , at  $\tau_{\rm gel}$  or  $\tau_{\rm end}$  is shown in Fig. 14(c). For

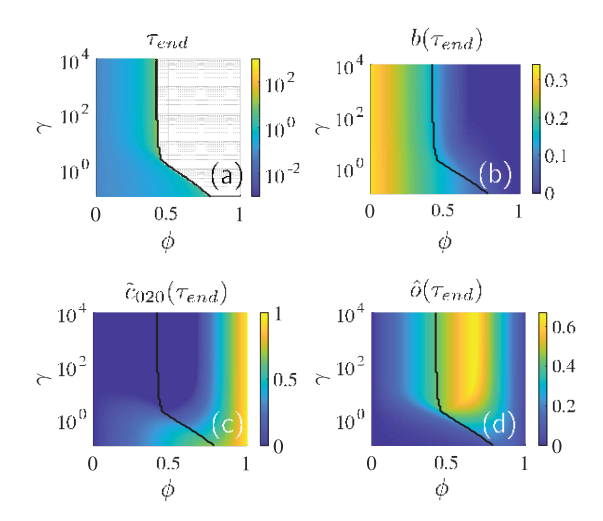


FIG. 14. (Case 1) Fibrinogen binding rate  $\gamma$  and initial composition parameter  $\varphi$  are varied with branching rate  $\kappa = 10$ . To the left of the black line, a gel forms. (a)  $\tau_{\rm end}$ , and concentrations at  $\tau_{\rm end}$  of (b) branch points b, (c) fibrinogen monomer  $\tilde{c}_{020}$ , and (d) fibrinogen in oligomer  $\hat{o}$  at  $\tau_{\rm gel}$  or at  $\tau_{\rm end} = 10^{10}$  with no conversion.

a given  $\varphi$  value, this concentration is lower in the no-gel region than in the gel region. When no gel forms, fibrinogen monomer has a long time to become incorporated into oligomers, and this results in a lower fibrinogen monomer concentration than when a gel does form. Additionally, the concentration  $\tilde{c}_{020}$  approaches 1 as  $\varphi \to 1$ . With low or no fibrin, few or no oligomers can form and fibrinogen remains in monomer form.

Figure 14(d) shows the dependence of the fibrinogen in oligomer concentration on  $\gamma$  and  $\varphi$ . The largest concentration of fibrinogen in oligomers occurs for  $\varphi \approx 0.66$ . At this  $\varphi$  value, there are approximately two fibrinogen monomers for every fibrin monomer. For fibrinogen binding rate  $\gamma = 1$  or higher, we expect that many of the oligomers present are "inert" trimers composed of two fibrinogen monomers and one fibrin monomer, the species we denote by  $C_{120}$ . That this is indeed the case is indicated by the fact that  $\tilde{o} \approx 0.66$  for  $\gamma > 10$  when  $\varphi = 0.66$ .

The insensitivity of the gel/no-gel boundary to  $\gamma$  when  $\gamma$  is sufficiently large can be explained by looking at the terms that dominate at early times in the equations for the free fibrin reaction site and fibrinogen monomer concentrations. These are

$$\frac{d\tilde{c}_{020}}{d\tau} \approx \frac{dr}{d\tau} \approx -2\gamma \,\tilde{c}_{020}r. \tag{E1}$$

We note that  $\tilde{c}_{020}(0) = \varphi$  and  $r(0) = 2(1 - \varphi)$  imply that  $\tilde{c}_{020}(0) = 3\varphi - 2 + r(0)$ , and that it follows that  $\tilde{c}_{020}(\tau) = 3\varphi - 2 + r(\tau)$  for  $\tau \ge 1$  because  $\tilde{c}_{020}$  and r decrease at the same rate. Substituting this expression for  $\tilde{c}_{020}(\tau)$  into the differential equation for  $r(\tau)$  and solving the resulting equation gives

$$r(\tau) = \frac{2 - 3\varphi}{1 + \nu(\tau)^{\frac{1}{2}} \frac{2\varphi - 2}{\varphi} c_{\frac{2}{3\varphi - 2}}},$$
 (E2)

where  $v(\tau) = \exp[-2\gamma\tau(2-3\varphi) - \frac{3\varphi}{3\varphi-2}\log(\frac{2\varphi-2}{\varphi})]$ .

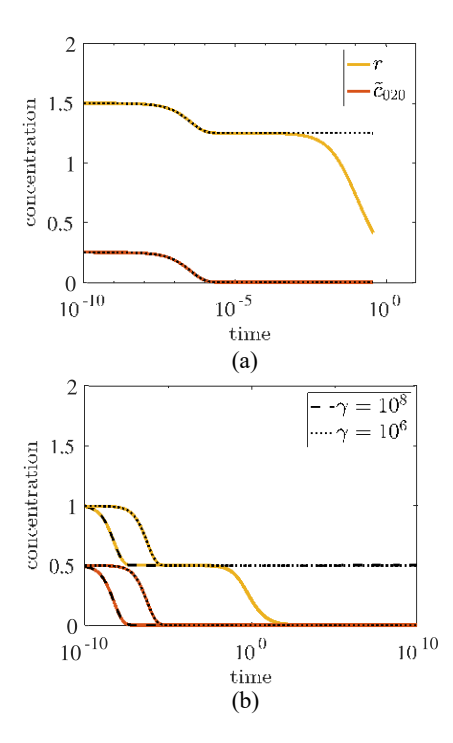


FIG. 15. (Case 1) Time course of  $r(\tau)$  and  $\tilde{c}_{020}$  for (a)  $\varphi = 1/4$  and (b)  $\varphi = 1/2$  with  $\kappa = 10$ . Dotted and dashed black lines correspond to plotting the approximate value for r and  $\tilde{c}_{020}$  using Eq. (E2) for  $\gamma = 10^6$  and  $\gamma = 10^8$ , respectively. Note the different x axis scales.

Figure 15 shows how the approximate value for  $r(\tau)$  from Eq. (E2), and the corresponding approximate  $\tilde{c}_{020}(\tau)$  (dashed black), compare with solutions of the full system. We show solutions with  $\gamma = 10^6$  for  $\varphi = 1/2$  (gelation does not occur) in Fig. 15(a) and for  $\varphi = 1/4$  (gelation does occur) in Fig. 15(b). For both  $\varphi$  values, we see excellent agreement between the approximate solution and the full solution. We also see that  $\tilde{c}_{020}$  goes rapidly to zero. In this large  $\gamma$  limit, the fibrinogen monomer quickly binds to the initial fibrin monomers. Since two fibringen monomers can bind to each fibrin monomer, and the initial concentration of fibring en is less than twice the initial concentration of fibrin, fibrinogen monomer is almost completely depleted in a very short time while simultaneously the concentration of free reaction sites drops. From the relation  $\tilde{c}_{020}(\tau) - r(\tau) = 3\varphi - 2$ , we see that when  $\tilde{c}_{020} \approx 0$ ,  $r(\tau) \approx 2 - 3\varphi$ , consistent with the curves in Fig. 15. The limiting value  $r(\tau) \approx 2 - 3\varphi$  does not depend on the value of y. Since the rapid depletion of fibringen monomer and reduction of r to 2 –  $3\varphi$  occurs for all sufficiently large values of  $\gamma$ , the subsequent dynamics, including whether a gel forms, are essentially the same for all large  $\nu$ .

# 2. Cases 2 and 3: Free reaction site and branch dependence on $\kappa$

To better show the difference between the end time concentrations of free reaction sites and branch points in Cases 2 and 3, depicted in Fig. 8, we show the end time concentrations as a function of  $\kappa$  in Fig. 16 for  $\gamma = 1$  and  $\eta_m = 1$ . These curves correspond to the gray vertical lines found in Fig. 8 in the manuscript. For Case 2, we see a quick rise in the

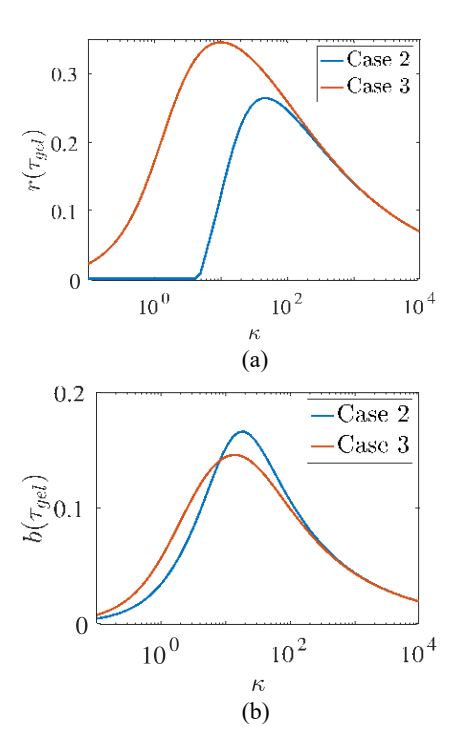


FIG. 16. End time concentration of (a) free reaction sites and (b) branch points for Case 2 (red) and Case 3 (blue) with  $\gamma = 1$ ,  $\eta_m = 1$ .

end time free reaction site concentration in Fig. 16(a) around  $\kappa \approx 3$ , corresponding to the beginning of the gel region. This rise contributes to the large increase in end time branch point concentration shown in Fig. 16(b). Interestingly, the peak end time branch concentration for Case 2 is larger than that for Case 3 even though the peak end time reaction site concentration is larger for Case 3 than Case 2.

# 3. Case 2: Effects of $\gamma$ and $\eta_m$ variations

We investigate the simulation end times and end time concentrations for Case 2 when varying  $\kappa$ ,  $\eta_m$ , and  $\gamma$  in Fig. 17. Figure 17(a) shows changes in  $\tau_{gel}$  as  $\gamma$  and  $\eta_m$  are varied, with gelation occurring to the right of the separatrix. As  $\gamma$ increases, the minimum value of  $\eta_m$  needed for gelation also increases, as faster fibrin monomer production is needed to compete with the faster fibrinogen binding. In Fig. 17(b), we see that branch formation is strongly limited in the no-gel region, and, in the gel region, the end time branch concentration increases as  $\eta_m$  increases. Figure 17(c) shows that there is very little fibringen monomer at gel time, and that the amount of fibringen monomer concentration at gel time decreases as  $\eta_m$ increases with  $\gamma$  fixed. In the no-gel region of Fig. 17(c), the end time fibrinogen monomer concentration is very low and corresponds to the high end time concentration of fibringen in oligomer found in the no-gel region of Fig. 17(d).

#### 4. Case 2: Relative timescales

We examine the time course of model variables and of fibrin reaction site production and consumption for a base case ( $\gamma = 1$ ,  $\kappa = 10$ ,  $\eta_m = 1$ ,  $\eta_o = 0$ ) and six other cases in

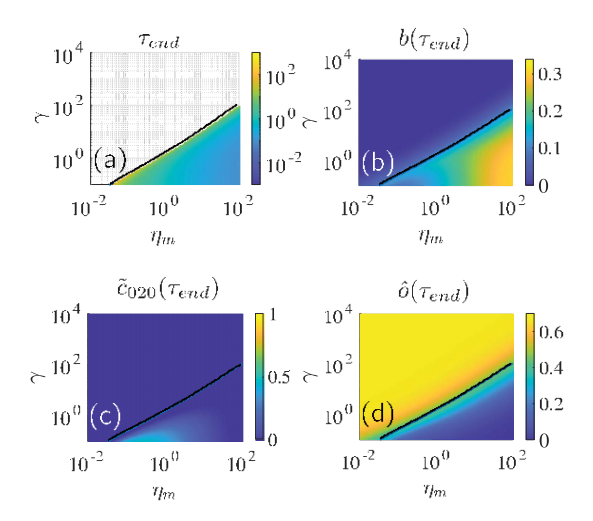


FIG. 17. (Case 2) Each concentration or gel time is a function of monomeric conversion rate  $\eta_m$  and varying  $\gamma$ , fixed  $\kappa = 10$ . (a) Gel time  $\tau_{\rm gel}$  and concentrations of (b) branches b, (c) fibrinogen monomer  $\tilde{c}_{020}$ , and (d) fibrinogen in oligomer  $\hat{o}$  at end of simulation. Black curves show the gel/no-gel boundary.

which, one at a time, we increase or decrease each of these parameters by 10-fold relative to its base case value. As shown in Fig. 18, the base case parameter values correspond to a point (the point labeled "2") that is in the gel region but close to the gel/no-gel boundary (for  $\gamma = 1$ ). For each parameter, the 10-fold variation in one direction moves the parameter trio ( $\gamma$ ,  $\kappa$ ,  $\eta_m$ ) further into the gel region, while the variation in the other direction moves it into the no-gel region. The relative size of the terms contributing to changes of the reaction site concentration  $r(\tau)$  are key to understanding the results. Here, for convenience is Eq. (26) from the main paper:

$$\frac{dr}{d\tau} = -r^2 - \frac{\kappa}{2}r^3 - 2\gamma \tilde{c}_{020}r + 2\eta_m \tilde{c}_{020} + \eta_o \hat{o}, \tag{26}$$

For Case 2 simulations,  $\eta_o = 0$ , and so reaction sites are produced only by conversion of fibrinogen monomers to fibrin and they are "consumed" in forming branches, forming links, and binding to fibrinogen. In the simulations shown below, the main determinants of whether a gel forms come from the inequalities in Eq. (36) of the main paper reproduced here:

$$\frac{^{3}}{\kappa^{020}} \frac{4\gamma \,\tilde{c}}{\kappa^{020}} \,^{1/2} < r < \frac{\eta_{m}}{\nu}. \tag{36}$$

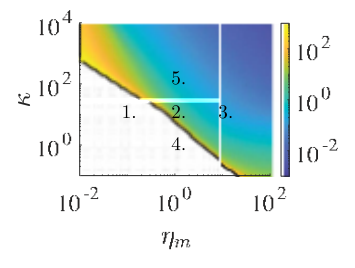


FIG. 18. (Case 2) Heatmap of  $\tau_{\rm end}$  for various  $\eta_m$  and  $\kappa$  values with  $\gamma = 1$ . The base case considered here is point "2" and has  $\eta_m = 1$ ,  $\kappa = 10$ , and  $\gamma = 1$ .

With  $\eta_o = 0$  and r(0) = 0, we see from Eq. (26) that  $r(\tau)$  6  $\eta_m/\gamma$  is always true because production of reaction sites by fibrinogen conversion must at least match their consumption through fibrinogen binding. But the amount by which  $\eta_m$  exceeds  $\gamma r$  determines how many "surplus" reaction sites are available for branch or link formation. The left inequality concerns the relative rates of using reaction sites to form branches or for fibrinogen binding. From all of our examples, it is clear that this inequality must hold for a significant portion of a simulation if a gel is to form. It is also useful, particularly to understand the nongelling cases, to compare two additional pairs of terms from Eq. (26). When  $\frac{2}{r} < r$ , the rate of branch formation is greater than the rate of fink formation, and when  $2\gamma \tilde{c}_{020} < r$ , the rate of link formation exceeds that of fibrinogen binding.

In Fig. 19 we look at the effect of the 10-fold changes in the fibringen monomer conversion rate coefficient  $\eta_m$ . The relevant parameter values are indicated by points "1" and "3" on the heatmap in Fig. 18. In Figs. 19(a) and 19(d) we see that for  $\eta_m = 0.1$ , gelation does not occur. In the right inequality in Eq. (36),  $\eta_m/\gamma = 0.1$  and is only a little greater than  $r(\tau)$  for a significant part of the simulation. The left inequality is not satisfied until  $\tau \approx 12$  when most of the fibringen has been depleted. Neither the concentration of fibrin monomer  $\tilde{c}_{102}$  nor the concentration of reaction sites r ever becomes large. Figure 19(d) shows that by the time fibrinogen is depleted, about 35% of the fibringen has been converted to fibrin monomers and most of the rest of the fibrinogen has bound with the fibrin monomers to form inert trimers. In Fig. 19(a), we see that fibring binding has neutralized most of the reaction sites produced by fibrinogen's conversion to fibrin, some of the fibrin has formed links with other fibrin monomers, and little branch formation has occurred. Figure 22(a) shows that for this simulation,  $r(\tau)$  is less than half of <sup>2</sup> throughout the simulation, showing that link formation is strongly favored over branch formation, and that  $r(\tau)$  is much less than  $2\nu \tilde{c}_{020}$  for almost all of the simulation, indicating that fibrinogen binding to reaction sites is strongly favored over link formation. These relations explain the ordering of fibrin reactions site consumption seen in Fig. 19(a).

We see in Fig. 19(e) for  $\eta_m = 1$ , that  $r(\tau)$  is greater than the lower limit in Eq. (36) starting at a time coinciding with the beginning of rapid branch formation. From Fig. 19(b), we see that at  $\tau_{\rm gel}$  the consumption of reaction sites through branch formation slightly exceeds their consumption through fibrinogen binding and their consumption through link formation. At  $\tau_{\rm gel}$ , the concentration of inert trimers is less than one-half the concentration of branches.

Figures 19(c) and 19(f) show results for  $\eta_m = 10$ . The gel forms much more quickly than for  $\eta_m = 1$ . The reaction site concentration r is far below the upper limit from Eq. (36) for the entire simulation so that many more reactions sites are produced than are used for fibrinogen binding. We see that r is above the lower limit from an early time coinciding with the onset of rapid branch formation. That r so quickly exceeds  $\frac{4\gamma \bar{c}_{020}/\kappa}{\epsilon_{020}/\kappa}$  is a consequence of the rapid increase in r and drop in  $\tilde{c}_{020}$  both of which are due to the rapid conversion of fibrinogen to fibrin. Even though a gel forms quickly, most of the fibrinogen has been converted to fibrin monomers by  $\tau_{\rm gel}$ , and a little less than half of the reaction sites on these

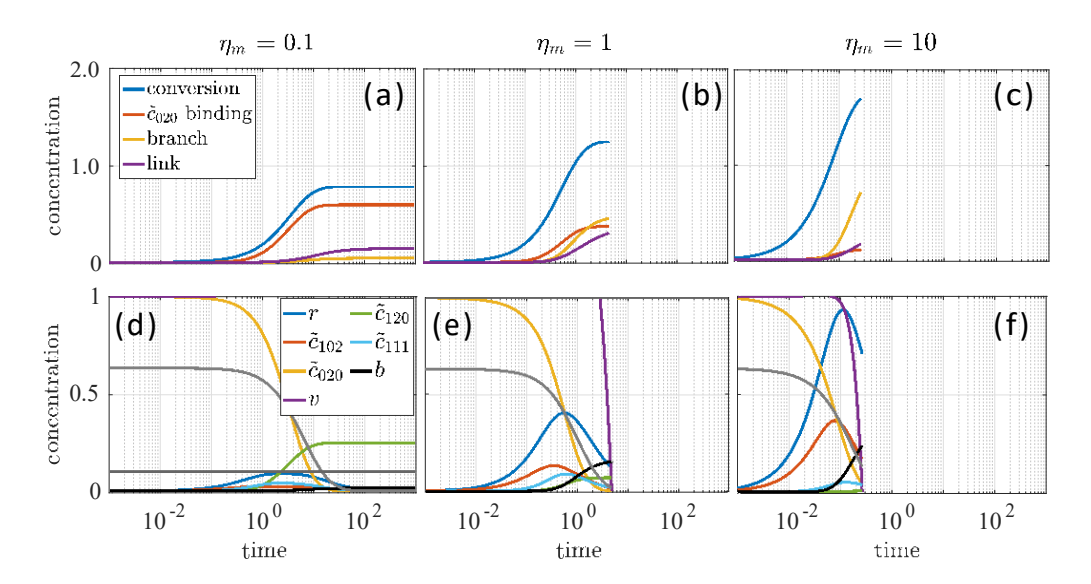


FIG. 19. (Case 2) Variations in  $\eta_m$ . Time course of the integral of the individual terms in that contribute to  $r(\tau)$  (top row) and time course of the concentrations of fibrinogen monomers ( $\tilde{c}_{020}$ ), fibrin monomers ( $\tilde{c}_{102}$ ), fibrinogen-fibrin dimers ( $\tilde{c}_{111}$ ), inert trimers ( $\tilde{c}_{120}$ ), free fibrin reaction sites (r), branch points (b), and gel indicator function v (bottom row) for three  $\eta_m = 0.1$ , 1.0, 10.0 values with  $\kappa = 10$ ,  $\gamma = 1$ . The gray dotted lines refer to upper and lower bounds on r in Eq. (36).

monomers have gone into branch formation, far exceeding the portion of reaction sites used for link formation or blocked by fibrinogen binding.

In Fig. 20 we look at the effect of the 10-fold changes in  $\kappa$ . The relevant parameter values are indicated by points "4" and "5" on the heatmap in Fig. 18. In Figs. 20(a) and 20(d) we see that for  $\kappa = 1$ , gelation does not occur. For the entire simulation, r is substantially below the upper limit  $\eta_m/\gamma = 1$ , indicating that a significant fraction of the reaction sites produced by fibrinogen conversion are available for branch or link formation. However, r is also below  $\frac{1}{4\gamma \tilde{c}_{020}/\kappa}$ , which starts at the relatively high value of 2, for much of the

simulation, and fibrinogen binding is strongly favored over branch formation. Because of the low branching rate coefficient  $\kappa$ , r is far below the level  $2/\kappa$  for the entire simulation, as shown in Fig. 22(b), so link formation is also greatly favored over branch formation. That figure also shows that r is substantially above  $2\gamma\tilde{c}_{020}$  starting a little after  $\tau=1$ , implying that link formation happens at a much faster rate than fibrinogen binding. These results explain both the large fraction of reaction sites that are used for link formation rather than fibrinogen binding and the very low consumption of reaction sites for branch formation. The diversion of reaction sites to link formation rather than fibrinogen binding has the

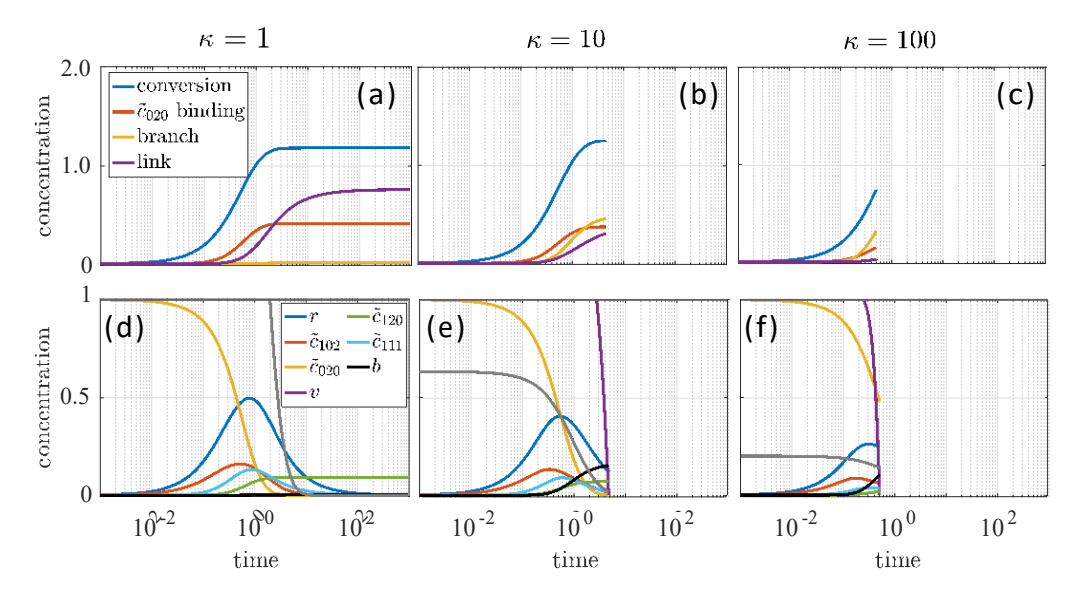


FIG. 20. (Case 2) Variations in  $\kappa$ . Time course of the integral of the individual terms in that contribute to  $r(\tau)$  (top row) and time course of the concentrations of fibrinogen monomers ( $\tilde{c}_{020}$ ), fibrin monomers ( $\tilde{c}_{102}$ ), fibrinogen-fibrin dimers ( $\tilde{c}_{111}$ ), inert trimers ( $\tilde{c}_{120}$ ), free fibrin reaction sites (r), branch points (b), and gel indicator function v (bottom row) for three  $\kappa = 1$ , 10, 100 values with  $\eta_m = 1$ ,  $\gamma = 1$ . The gray dotted lines refer to upper and lower bounds on r in Eq. (36).

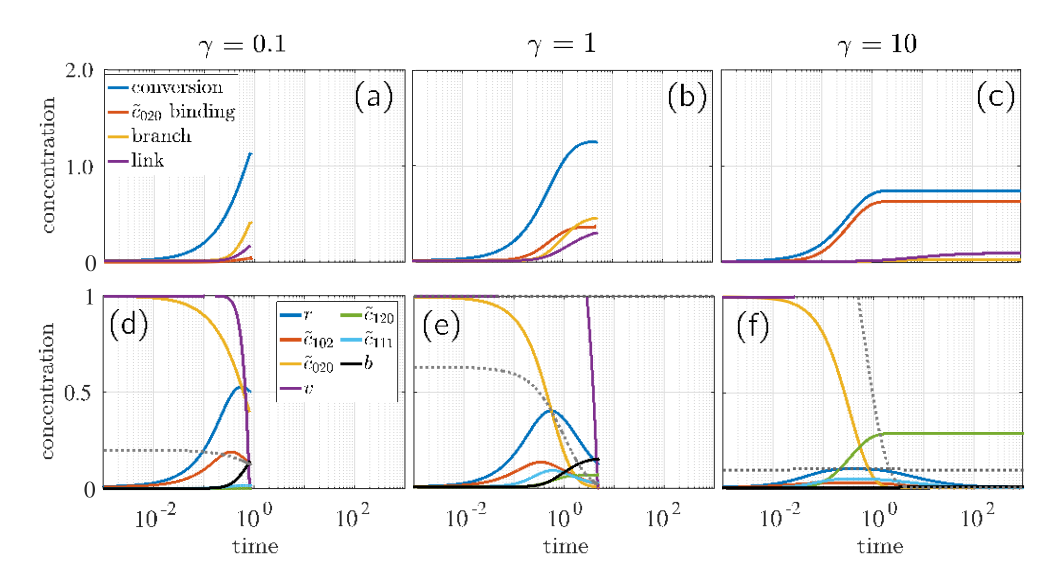


FIG. 21. (Case 2) Variations in  $\gamma$ . Time course of the integral of the individual terms in that contribute to  $r(\tau)$  (top row) and time course of the concentrations of fibrinogen monomers ( $\tilde{c}_{020}$ ), fibrin monomers ( $\tilde{c}_{102}$ ), fibrinogen-fibrin dimers ( $\tilde{c}_{111}$ ), inert trimers ( $\tilde{c}_{120}$ ), free fibrin reaction sites (r), branch points (b), and gel indicator function v (bottom row) for three v = 0.1, 1, 10 values with  $\eta_m = 1$ ,  $\kappa = 10$ . The gray dotted lines refer to upper and lower bounds on r in Eq. (36).

consequence that the concentration of inert trimers at the end of the simulation, shown in Fig. 20(d), is lower than it is for the other nongelling cases,  $\eta_m = 0.1$  in Fig. 19(d) and  $\gamma = 10$  in Fig. 21(f).

Figures 20(b) and 20(e) show that for  $\kappa = 10$ , our base case, comparable amounts of the fibrin reaction sites produced by conversion of fibrinogen are used in branch formation, fibrinogen binding, and link formation, and the final concentration of inert trimers is small. For  $\kappa = 100$  [Figs. 20(c) and 20(f)], r quickly exceeds  $\frac{1}{4\gamma \tilde{c}_{020}/\kappa}$ , which starts at the relatively low value of 0.2, branch formation occurs rapidly, and gelation happens early. In this simulation with a moderate rate of fibrinogen conversion and rapid rate of branch formation, almost half of the fibrinogen monomers remain at  $\tau_{\rm gel}$ .

Figure 21 shows the effects of 10-fold changes in  $\gamma$ . These changes correspond to movement in the  $\eta_m$ ,  $\kappa$ ,  $\gamma$  parameter space perpendicular to the plane of the heatmap shown in

Fig. 18. Compared to the location of the gel/no-gel boundary in Fig. 18, the gel/no-gel boundary is lower and further to the left for y = 0.1, and higher and further to the right for y= 10 (not shown). Figure 21(f) shows that gelation does not happen for y = 10. Figure 21(c) shows that the rate of fibringen binding to the fibrin reaction sites almost matches their rate of production by conversion of fibrinogen; correspondingly, for much of the simulation, r is approximately equal to the upper limit in Eq. (36). The rates, of branch formation and link formation remain low, as r 
iand  $r 
i 2\nu \tilde{c}_{020}$  (see Fig. 22) until most of the fibringen has been depleted. Approximately 75% of the original fibrinogen has been incorporated into inert trimers by the time fibrinogen is depleted. With y = 1 (the base case), shown in Figs. 21(b) and 21(e), gelation occurs and branch formation accounts for slightly more reaction site utilization than does fibrinogen binding. Figure 21(d) shows that when  $\gamma$  is dropped to 0.1, gel formation occurs quickly, occurring at about the same time as

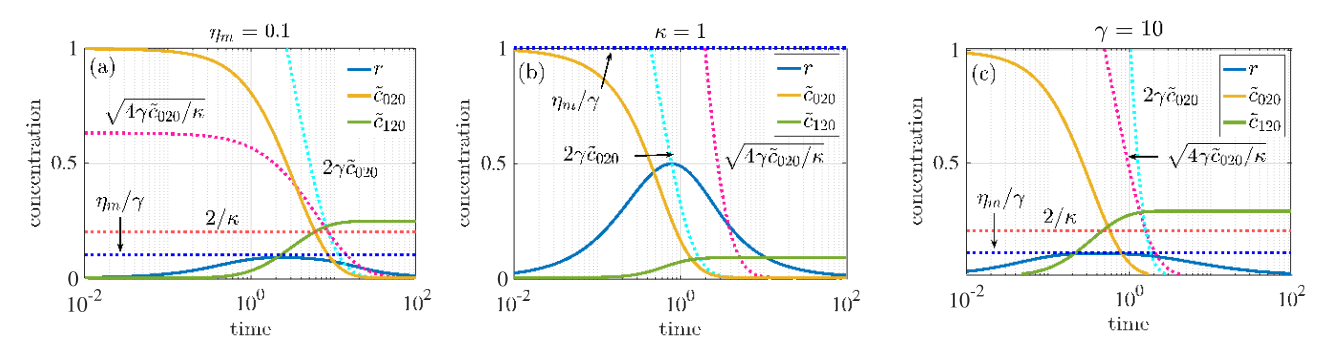


FIG. 22. (Case 2) Nongelling simulations: (a)  $\eta_m = 0.1$ ,  $\kappa = 10$ ,  $\gamma = 1$ , (b)  $\eta_m = 1$ ,  $\kappa = 1$ ,  $\gamma = 1$ , (c)  $\eta_m = 1$ ,  $\kappa = 10$ ,  $\gamma = 10$ . Time-course of concentrations of reactive sites r, fibrinogen monomers  $\tilde{c}_{020}$ , and inert trimers  $\tilde{c}_{120}$ . Plots of reaction rate boundary curves:  $r < \gamma$  if the rate of reaction site production by fibrinogen conversion exceeds the rate of reaction site use by fibrinogen binding, r > 1 if the rate of reactive site use for branch formation exceeds that by link formation, and  $r > 2\gamma \tilde{c}_{020}$  if the rate of reaction site use for link formation exceeds that by fibrinogen binding.

when  $\kappa = 100$  [Fig. 20(f)] and just a little later than it does when  $\eta_m = 10$  [Fig. 19(f)].

It is interesting to compare the parameter combinations in each set (Figs. 19–21) that lead to the fastest gelling. Among these simulations, the one with  $\eta_m = 10$  and baseline values of  $\kappa$  and  $\gamma$ , achieves the highest values r and  $\tilde{c}_{102}$ . The fibrin monomer concentration reaches its peak at the start of rapid branch formation, and r peaks about half-way though the interval of rapid branch formation that leads to gelation. Almost all of the fibrinogen has been depleted by  $\tau_{\rm gel}$ , and the use of reaction sites for branch formation far exceeds, by about fourfold, their use for either fibrinogen binding or link formation. The concentration of branches at gel time  $b(\tau_{\rm gel})$  is highest among the three fast-gelling cases. For the simulation with  $\gamma = 0.1$  and baseline values of  $\eta_m$  and  $\kappa$ , r and  $\tilde{c}_{102}$  reach moderate levels, with  $\tilde{c}_{102}$  and r again

peaking at the start of rapid branch formation and midway between the start of rapid branch formation and gel time, respectively. About 60% of the fibrinogen had been used by gel time. The value of  $b(\tau_{\rm gel})$  is lower than for the  $\eta_m = 10$  case. With  $\kappa = 100$  and  $\eta_m$  and  $\gamma$  at their baseline values, the timing of the peaks of  $\tilde{c}_{102}$  and r relative to the time interval of rapid branch formation is similar to the other cases, but the peaks in  $\tilde{c}_{102}$  and r are much smaller than in the previous two cases. At gel time, only  $\approx 50\%$  of the fibrinogen has been used. The consumption of reaction sites in branch formation is about twice that for fibrinogen binding which, in turn, is much larger than their use for link formation. The value  $b(\tau_{\rm gel})$  is much lower than that for  $\eta_m = 10$  and somewhat lower than for  $\gamma = 0.1$ , and this likely reflects the differing levels of fibrinogen depletion by gel time in the three cases.

- E. A. Ryan, L. F. Mockros, J. W. Weisel, and L. Lorand, Structural origins of fibrin clot rheology, Biophys. J. 77, 2813 (1999).
- [2] J. W. Weisel, Fibrinogen and fibrin, Adv. Protein Chem. **70**, 247 (2005).
- [3] I. N. Chernysh and J. W. Weisel, Dynamic imaging of fibrin network formation correlated with other measures of polymerization, Blood 111, 4854 (2008).
- [4] J. W. Weisel and R. I. Litvinov, Mechanisms of fibrin polymerization and clinical implications, Blood, J. American Society Hematology 121, 1712 (2013).
- [5] B. Blombäck, K. Carlsson, K. Fatah, B. Hessel, and R. Procyk, Fibrin in human plasma: Gel architectures governed by rate and nature of fibrinogen activation, Thromb. Res. 75, 521 (1994).
- [6] A. L. Fogelson and J. P. Keener, Toward an understanding of fibrin branching structure, Phys. Rev. E 81, 051922 (2010).
- [7] C. L. Zapata-Allegro, Modeling of fibrin gelation dynamics and structure formation under flow, Ph.D. thesis, University of Utah, Salt Lake City, UT, 2018.
- [8] A. L. Fogelson, A. C. Nelson, C. Zapata-Allegro, and J. P. Keener, Development of fibrin branch structure before and after gelation, SIAM J. Appl. Math. 82, 267 (2022).
- [9] L. A. Chtcheglova, A. Haeberli, and G. Dietler, Force spectroscopy of the fibrin(ogen)–fibrin interaction, Biopolymers 89, 292 (2008).
- [10] M. Rocco, S. Bernocco, M. Turci, A. Profumo, C. Cuniberti, and F. Ferri, Early events in the polymerization of fibrin, Ann. N.Y. Acad. Sci. 936, 167 (2001).
- [11] J. L. Usero, C. Izquierdo, F. J. Burguillo, M. G. Roig, A. del Arco, and M. A. Herraeza, Kinetic analysis of the fibrin monomers aggregation: Calculation of the fibrinogen-fibrin equilibrium constant, Int. J. Biochem. 13, 1191 (1981).
- [12] A. Henschen, On the identity of fibrin(ogen) oligomers appearing during fibrin polymerization, in *Fibrinogen, Thrombosis, Coagulation, and Fibrinolysis* (Springer, Berlin, 1990), pp. 49–53.
- [13] R. M. Ziff and G. Stell, Kinetics of polymer gelation, J. Chem. Phys. 73, 3492 (1980).
- [14] M. Rubinstein and R. H. Colby, *Polymer Physics* (Oxford University Press, New York, 2003).

- [15] R. R. Hantgan and J. Hermans, Assembly of fibrin: A light scattering study, J. Biol. Chem. 254, 11272 (1979).
- [16] J. W. Weisel and C. Nagaswami, Computer modeling of fibrin polymerization kinetics correlated with electron microscope and turbidity observations: Clot structure and assembly are kinetically controlled, Biophys. J. 63, 111 (1992).
- [17] R. D. Guy, A. L. Fogelson, and J. P. Keener, Fibrin gel formation in a shear flow, Math. Med. Biol.: J. IMA 24, 111 (2007).
- [18] G. Th. Guria, M. A. Herrero, and K. E. Zlobina, A mathematical model of blood coagulation induced by activation sources, Discrete Cont. Dynam. Syst. A 25, 175 (2009).
- [19] O. S. Rukhlenko, O. A. Dudchenko, K. E. Zlobina, and G. Th. Guria, Mathematical modeling of intravascular blood coagulation under wall shear stress, PLoS ONE 10, e0134028 (2015).
- [20] M. C. Naski and J. A. Shafer, A kinetic model for the alphathrombin-catalyzed conversion of plasma levels of fibrinogen to fibrin in the presence of antithrombin III, J. Biol. Chem. 266, 13003 (1991).
- [21] S. Yesudasan, X. Wan, and R. D. Averett, Coarse-grained molecular dynamics simulations of fibrin polymerization: Effects of thrombin concentration on fibrin clot structure, J. Mol. Model. 24, 109 (2018).
- [22] S. Yesudasan, X. Wan, and R. D. Averett, Fibrin polymerization simulation using a reactive dissipative particle dynamics method, Biomech. Model. Mechanobiol. 17, 1389 (2018).
- [23] A. C. Nelson, M. A. Kelley, L. M. Haynes, and K. Leiderman, Mathematical models of fibrin polymerization: Past, present, and future, Curr. Opin. Biomed. Eng. 20, 100350 (2021).
- [24] A. L. Fogelson and J. P. Keener, A framework for exploring the post-gelation behavior of Ziff and Stell's polymerization models, SIAM J. Appl. Math. 75, 1346 (2015).
- [25] E. P. Brass, W. B. Forman, R. V. Edwards, and O. Lindan, Fibrin formation: The role of the fibrinogen-fibrin monomer complex, Thromb. Haemost. 36, 037 (1976).
- [26] J. Wilf and A. P. Minton, Soluble fibrin-fibrinogen complexes as intermediates in fibrin gel formation, Biochemistry 25, 3124 (1986).

- [27] G. Marx, Simulating fibrin clotting time, Med. Biol. Eng. Comput. 44, 79 (2006).
- [28] A. C. Nelson, J. P. Keener, and A. L. Fogelson, Kinetic model of two-monomer polymerization, Phys. Rev. E 101, 022501 (2020).
- [29] D. T. Gillespie, A general method for numerically simulating the stochastic time evolution of coupled chemical reactions, J. Comput. Phys. 22, 403 (1976).
- [30] D. T. Gillespie, Exact stochastic simulation of coupled chemical reactions with delays, J. Phys. Chem. 81, 2340 (1977).
- [31] A. A. Onasoga-Jarvis, T. J. Puls, S. K. O'Brien, L. Kuang, H. J. Liang, and K. B. Neeves, Thrombin generation and fibrin formation under flow on biomimetic tissue factor-rich surfaces, J. Thromb. Haemost. 12, 373 (2014).
- [32] K. C. Gersh, K. E. Edmondson, and J. W. Weisel, Flow rate and fibrin fiber alignment, J. Thromb. Haemost. 8, 2826 (2010).
- [33] A. S. Wolberg, Thrombin generation and fibrin clot structure, Blood Rev. 21, 131 (2007).
- [34] J. W. Weisel, Structure of fibrin: Impact on clot stability, J. Thromb. Haemost. **5**, 116 (2007).